JCI The Journal of Clinical Investigation

Apobec1 complementation factor overexpression promotes hepatic steatosis, fibrosis and hepatocellular cancer

Valerie Blanc, … , Lewis R. Roberts, Nicholas O. Davidson

J Clin Invest. 2020. https://doi.org/10.1172/JCI138699.

Research In-Press Preview **Hepatology** **Metabolism**

Graphical abstract

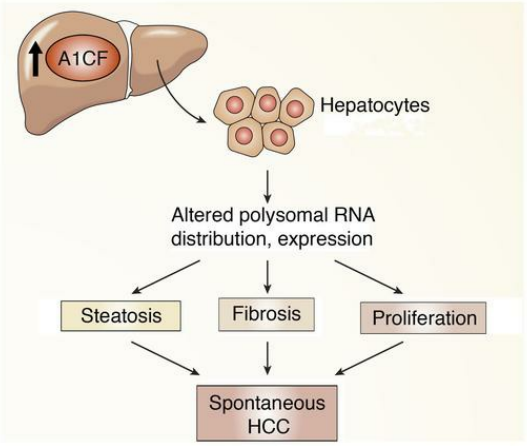

Graphical abstract

Apobec1 complementation factor overexpression promotes hepatic steatosis, fibrosis and hepatocellular cancer.

Valerie Blanc[1], Jesse D. Riordan[2], Saeed Soleymanjahi[1], Joseph H. Nadeau[2], ILKe Nalbantoglu[3], Yan Xie[1], Elizabeth A. Molitor[1], Blair B. Madison[1], Elizabeth M. Brunt[4], Jason C. Mills[1], Deborah C. Rubin[1], Irene O. Ng[5], Yeonjung Ha[6], Lewis R. Roberts[6] and Nicholas O. Davidson[1,7]

[1]Division of Gastroenterology, Washington University School of Medicine, Saint Louis, MO 63110, [2]Pacific Northwest Research Institute, Seattle, WA 98122, [3]Department of Pathology, Yale University School of Medicine, New Haven, CT 06520, [4]Department of Pathology and Immunology, Washington University School of Medicine, Saint Louis, MO 63110, [5]Department of Pathology and State Key Laboratory of Liver Research, Li Ka Shing Faculty of Medicine, The University of Hong Kong, Hong Kong, China, [6]Department of Medicine, Mayo Clinic College of Medicine and Science, Rochester, MN 55902

To whom correspondence should be addressed[7]:
Nicholas O. Davidson, MD, DSc
Gastroenterology Division,
Washington University School of Medicine
Saint Louis, MO 63110
314-362-2027
Email: nod@wustl.edu

Current addresses:
J.D. Riordan, University of Iowa, Iowa City, IA 52242
J.H. Nadeau, Maine Medical Center Research Institute, Scarborough, ME 04074
Y. Ha, CHA Bundang Medical Center, CHA University, Gyeonggi-do, Korea
B.B. Madison, Poseida Therapeutics, Inc, San Diego, CA 92921

The authors have declared that no conflict of interest exists

Keywords: RNA binding protein; polysomal RNA; hepatocellular cancer; ApolipoproteinB

ABSTRACT

RNA binding protein Apobec1 Complementation Factor (A1CF) regulates posttranscriptional *ApoB* mRNA editing but the range of RNA targets and long-term impact of altered A1CF expression on liver function are unknown. Here we studied hepatocyte-specific *A1cf* transgenic (*A1cf* $^{+/Tg}$), *A1cf*$^{+/Tg}$ *Apobec1*$^{-/-}$ and *A1cf* $^{-/-}$ mice fed chow or high fat/high fructose diets using RNA-Seq, RNA-CLIP Seq and tissue microarrays from human hepatocellular cancer (HCC). *A1cf* $^{+/Tg}$ mice exhibited increased hepatic proliferation and steatosis, with increased lipogenic gene expression (*Mogat1*, *Mogat2*, *Cidea*, *Cd36*) associated with shifts in polysomal RNA distribution. Aged *A1cf* $^{+/Tg}$ mice developed spontaneous fibrosis, dysplasia and HCC, which was accelerated on a high fat/fructose diet and independent of *Apobec1.* RNA-Seq revealed increased expression of mRNAs involved in oxidative stress (*Gstm3*, *Gpx3*, *Cbr3*), inflammatory response (*Il19*, *Cxcl14*, *Tnf*α, *Ly6c*), extracellular matrix organization (*Mmp2*, *Col1a1*, *Col4a1*), proliferation (*Kif20a*, *Mcm2*, *Mcm4*, *Mcm6*) with a subset of mRNAs (including *Sox4*, *Sox9*, *Cdh1*) identified in RNA CLIP-Seq. Increased A1CF expression in human HCC correlated with advanced fibrosis and with reduced survival in a subset with nonalcoholic fatty liver disease. In conclusion, we show that hepatic A1CF overexpression selectively alters polysomal distribution and mRNA expression, promoting lipogenic, proliferative and inflammatory pathways leading to HCC.

Non-standard Abbreviations

Nonalcoholic fatty liver disease: NAFLD

Nonalcoholic steatohepatitis: NASH

Hepatocellular cancer: HCC

ApolipoproteinB: APOB

Apobec1 complementation factor: A1CF

Introduction

The increasing worldwide prevalence of nonalcoholic fatty liver disease (NAFLD) is projected to result in a corresponding increase in major progressive outcomes, including nonalcoholic steatohepatitis (NASH), fibrosis and hepatocellular cancer (HCC) (1). Those comorbid complications of NAFLD represent a pressing concern, particularly with the emergence of HCC as an increasingly common worldwide cause of cancer-associated mortality (2). In addition, because NAFLD progression is associated with a range of other comorbidities including cardiovascular disease (the leading cause of death among patients with NAFLD (3)), there is also an increasing need to understand the role of both genetic and environmental modifiers in the etiology and progression of those important comorbidities. Among the genes identified in NAFLD susceptibility, several have been implicated in HCC development, including *TM6SF2*, *PNPLA3*, *MBOAT7* and *APOB*, suggesting that alterations in genes that regulate critical pathways in hepatic lipid compartmentalization and/or VLDL secretion may play key roles in both NAFLD development as well as in disease progression (4). In relation to NAFLD and cardiovascular disease risk, the E167K variant of TM6SF2 (rs 58542929 C/T) is an important modifier of both blood lipid levels and hepatic steatosis, with the rare T variant conferring protection against cardiovascular disease because of reduced hepatic VLDL secretion but with a consequence of increased steatosis and NAFLD development (5).

The association of cardiovascular disease and NAFLD has fueled interest in the mechanisms regulating hepatic apolipoproteinB (APOB) and VLDL production in humans, including the possibility that therapeutic targeting of VLDL secretion might offer clinical utility as a strategy for lowering plasma lipid levels. While some reports suggest that antisense targeting of APOB might be feasible without the adverse effects of hepatic steatosis (6), the predominant clinical experience suggests that reducing lipid levels by inhibiting VLDL secretion also promotes hepatic steatosis (7, 8), although the long term consequences are still unknown. Other studies

have demonstrated a role for epigenetic or posttranscriptional gene regulation of APOB expression, including a role for Apobec1 complementation factor (A1CF), an AU-rich RNA binding protein, identified in earlier screens for genetic complementation of C-to-U RNA editing activity of the cytidine deaminase APOBEC1 (9, 10). A1CF is widely expressed in both human and mouse tissues, including at high levels in the liver where it binds a range of RNAs, including *ApoB* and *Il-6* (11). *A1cf* null mice revealed distinctive alterations in APOBEC1-dependent C-to-U RNA editing, yet those mice revealed no change in hepatic *ApoB* mRNA editing or expression (12, 13). However, neither of those studies examined the impact of *A1cf* deletion on the regulation of hepatic lipid metabolism or the longer-range impact for metabolic liver disease. Earlier studies showed hepatic A1CF was upregulated in *ob/ob* mice and that siRNA knockdown in hepatocytes impaired VLDL secretion (14). Those studies collectively raise the possibility that A1CF might exhibit both gain- and loss-of-function phenotypes in vivo, consistent with findings that an *A1CF* variant allele is a causal gene for regulating serum triglyceride levels in humans (15).

Here we report studies that address those unanswered questions. We generated liver-specific *A1cf* transgenic mice revealing a phenotype with spontaneous steatosis, fibrosis and HCC, none of which were observed in *A1cf* null mice. We identified a range of hepatic A1CF RNA targets and pathways, including oxidative stress, inflammation and extracellular matrix organization. Finally, we demonstrate that A1CF was overexpressed in a subset of patients with HCC. The findings collectively point to a new role for RNA binding protein A1CF in liver pathobiology in both mice and humans.

Results

A1cf $^{+/Tg}$ mice exhibit increased hepatocyte proliferation and a subtle shift in VLDL secretion:

We generated two *A1cf* $^{+/Tg}$ founder lines (Supplemental Figure 1) with similar expression of the transgene (~2-3 fold above endogenous, Figure 1A), localized predominantly in hepatocyte nuclei (Supplemental Figure1A). Young (8-14 week), chow-fed *A1cf* $^{+/Tg}$ mice revealed elevated liver-to-body weight ratios and injury reflected by a 2-fold increased serum ALT (Figure1B), with no change in AST. We observed increased BrdU-positive hepatocytes in *A1cf* $^{+/Tg}$ mice (Figure1B and Supplemental Figure1B) with increased Alpha fetoprotein (*Afp*) mRNA, consistent with increased proliferation (Supplemental Figure 1B). There were more lipid droplets in *A1cf* $^{+/Tg}$ mice with increased hepatic TG content (Figure1C). Hepatic and serum total cholesterol and fatty acids were unaltered in *A1cf* $^{+/Tg}$ mice (Supplemental Figure 1C). Fasting serum TG were comparable in both genotypes after a 4h fast (Figure 1D) but *A1cf* $^{+/Tg}$ mice showed no increase following a 16h fast compared to controls (Figure 1D and Supplemental Figure 1C), suggesting subtle impairment of VLDL secretion (16). We also found relatively increased APOB100 in livers of *A1cf* $^{+/Tg}$ mice, along with a shift of *ApoB* mRNA into actively translating polysomal fractions (Figure 1E), further suggesting impaired VLDL assembly and secretion in those mice. Fractionation of serum indicated a shift into smaller TG and cholesterol containing VLDL fractions (Figure 2A), with smaller nascent VLDL particles visualized in *A1cf* $^{+/Tg}$ mice (Figure 2A). In addition, studies in isolated hepatocytes revealed decreased secretion of APOB from *A1cf* $^{+/Tg}$ mice (Figure 2B), even though in vivo VLDL-TG secretion rates were comparable in both genotypes after either 4h or 16h fast (Supplemental Figure 1D). These data collectively suggest that hepatic *A1cf* overexpression results in decreased APOB secretion associated with a shift in VLDL secretion towards smaller particles.

Prompted by findings showing that *A1cf* deletion in liver-like hepatoma cells decreased APOB secretion (15), we examined hepatic and serum lipid metabolism in *A1cf*$^{-/-}$ mice. However, we found no significant changes in serum or hepatic TG or cholesterol content and no change in VLDL secretion or in serum or hepatic APOB content or isoform distribution in *A1cf*$^{-/-}$ mice (Supplemental Figure 2A-D). We generated two independent lines of HepG2 CRISPR-deleted *A1CF* null cells (17), which revealed ~30% decrease in both APOB synthesis and secretion (Supplemental Figure 2E, F). Taken together, these findings suggest that loss of *A1CF* slightly decreases APOB production in HepG2 cells but does not alter APOB expression or VLDL secretion in mouse liver.

_A1cf_$^{+/Tg}$ mice exhibit altered expression of genes promoting FA uptake and lipogenesis: We undertook RNA pathway analysis to understand the changes associated with the spontaneous hepatic steatosis observed in young *A1cf*$^{+/Tg}$ mice. Gene ontology revealed enrichment in genes involved in lipid biosynthesis (Figure 3A), including, *Cidea*, *Mogat1*, *Mogat2* and *Cd36* (18-20). Q-PCR revealed a 30-fold increase in *Cidea* and *Mogat1* mRNAs, a 10-fold increase in *Mogat2* mRNA and a 2-fold increase in *Cd36* mRNA (Figure 3B). We also observed increased MOGAT1 and MOGAT2 protein abundance in *A1cf*$^{+/Tg}$ liver (Figure 3C). Analysis of both *Cidea* and *Cd36* RNAs revealed a shift into actively translating polysomal fractions (Figure 4A), associated with ~3-fold increased CD36 and (qualitative) CIDEA protein expression (Figure 4B). Collectively, these results suggest that hepatic A1CF modulates genes involved in hepatic lipogenesis and FA utilization as well as hepatic VLDL assembly and secretion, conceivably by altering polysomal mRNA distribution and translation.

_A1cf_$^{+/Tg}$ mice develop hepatic fibrosis and spontaneous tumorigenesis, independent of APOBEC1 expression:

Aged (~12 month old) *A1cf* $^{+/Tg}$ mice exhibited increased fibrosis (Figure 5A) and fibrogenic mRNA expression, including α*Sma*, *Col1a1* and *Col4a1* (Figure 5A) with increased liver weight:body weight ratio (Supplemental Figure 3A) and increased serum ALT (Supplemental Figure 3A). In addition, there were visible tumors in 12/13 aged male *A1cf* $^{+/Tg}$ liver (Figure 5B) but none in aged (7/7) female *A1cf* $^{+/Tg}$ mice (data not shown). Because A1CF is a component of the C-to-U RNA editing machinery and since previous studies have demonstrated that APOBEC1 overexpression promotes promiscuous RNA editing and tumorigenesis (21, 22), we next asked if there was a requirement for APOBEC1 in the tumorigenesis observed in *A1cf* $^{+/Tg}$ mice. We generated a compound line of *A1cf* $^{+/Tg}$ *Apobec1*$^{-/-}$ mice which, at 12 months, exhibited increased liver:body weight ratio (Supplemental Figure 3A) and increased hepatic TG content, without changes in hepatic cholesterol or FA content (Supplemental Figure 3B), findings similar to 12 month old *A1cf* $^{+/Tg}$ mice. As expected, those *A1cf* $^{+/Tg}$ *Apobec1*$^{-/-}$ mice expressed only APOB100 (Supplemental Figure 3A). Those aged, male *A1cf* $^{+/Tg}$ *Apobec1*$^{-/-}$ mice also developed similar numbers of liver nodules when compared to *A1cf* $^{+/Tg}$ mice (Figure 5C) and again, similar to *A1cf* $^{+/Tg}$ mice, exhibited increased hepatocyte proliferation (Supplemental Figure 3C). Histopathologic analysis revealed that 5/10 aged *A1cf* $^{+/Tg}$ *Apobec1*$^{-/-}$ livers exhibited dysplastic nodules, with 1/5 HCC (Table 1) suggesting that A1CF-induced tumorigenesis is likely both APOBEC1 and RNA editing-independent. In addition, because liver-specific *A1cf* knockout mice exhibited aberrant alternative splicing of ketohexokinase-C RNA (23), a feature associated with HCC formation (24), we examined one year old male *A1cf* $^{-/-}$ mice but observed no spontaneous tumors (0/10 mice, Table 1, Supplemental Figure 4A). We observed increased hepatic TG content in 12-month old chow fed *A1cf* $^{-/-}$ mice, without changes in cholesterol or FA content, no change in transaminases but increased hepatic inflammatory marker mRNA expression for *Ly6c* and *Ccr2* (Supplemental Figure 4B, C). We will consider the significance of those findings in a later section, in the context of high fat, high fructose feeding.

Immunohistochemical analysis revealed heat shock protein 70 (HSP70), glypican 3 (GPC3) and p62 staining of tumor cells in both *A1cf* $^{+/Tg}$ and *A1cf* $^{+/Tg}$ *Apobec1*$^{-/-}$ mice (Figure 6A), with scattered inflammatory infiltrates, apoptotic and mitotic figures (Figure 6B). Despite the presence of hepatic steatosis and scattered inflammatory cells, there was no evidence of increased hepatic inflammation, based on lack of change in mRNA abundance for inflammation-associated genes in either genotype at 12 months (Supplemental Figure 5A). We also observed increased expression of β-CATENIN (both overall and nuclear, Figure 6C) as well as its downstream target CYCLIN D1 in the livers of aged *A1cf* $^{+/Tg}$ mice (Figure 6C). Those findings are relevant since activation of β-CATENIN is a key event in HCC (25).

Because of the progressive nature of liver tumorigenesis, we examined 6-month old chow fed, male *A1cf* $^{+/Tg}$ mice, which revealed small nodules in 4/7 mice. Those nodules revealed areas of steatosis, inflammation, hepatocyte ballooning and anisonucleosis but were not dysplastic (Supplemental Figure 5B). We also fed groups of male *A1cf* $^{+/Tg}$ and *A1cf* $^{-/-}$ mice a high fat, high fructose diet for 6 months in order to examine the impact of diet induced steatosis on hepatic tumorigenesis. Those findings revealed tumors in 9/14 *A1cf* $^{+/Tg}$ mice (Figure 7A and Table 2) and increased STAT3 activation with increased phospho-STAT3 expression (Figure 7B) along with increased expression of a known downstream target, *Hif1*α mRNA (26) (Figure 7C). We also observed immunohistochemical staining for GPC3 and HSP70 (Figure 7D) and increased expression of β-CATENIN (Figure 7E) in tumor nodules from *A1cf* $^{+/Tg}$ mice. By contrast and consistent with our observations in aged chow fed mice, no tumors were observed in high fat, high fructose fed *A1cf* $^{-/-}$ mice (Figure 7A) and there was no change in hepatic expression of β-CATENIN in those mice (Figure 7F). *A1cf* $^{-/-}$ mice exhibited comparable fibrotic injury to WT6NJ controls, with increased hepatic mRNA expression of *Col4a1* and *Spp1*, along with increased mRNA expression of several inflammatory genes (Supplemental Figure 6A, B), a

pattern similar to that alluded to above in 12 month old chow fed *A1cf* $^{-/-}$ mice (Supplemental Figure 4C). Those findings together, imply that the hepatic steatosis and inflammatory signaling observed in both chow-and high fat, high fructose fed *A1cf* $^{-/-}$ mice are insufficient to drive tumor initiation.

Transcriptome-wide analysis of *A1cf* $^{+/Tg}$ liver and isolated hepatocytes:

The findings to this point demonstrate that *A1cf* $^{+/Tg}$ mice exhibit alterations in mRNAs involved in hepatic lipogenic and VLDL assembly pathways, but raise questions regarding the mechanisms associated with the fibrogenic and tumorigenic phenotypes observed. As an approach to identify those pathways, we undertook RNA-Seq and STRING analysis (27) to examine functional enrichment and protein-protein interaction networks from whole liver transcriptomes in young (12 week) mice (Figure 8A). Those analyses revealed changes in several functional categories including cell cycle, extracellular matrix organization, TG metabolism and lipid particle organization as well as oxidative stress (Figure 8A). Q-PCR validated upregulation of several target mRNAs involved in these pathways (Figure 8B). The mRNA changes in regard to cell cycle and extracellular matrix organization extend findings illustrated above showing increased proliferation and fibrogenesis in *A1cf* $^{+/Tg}$ mice. We pursued the findings implicating altered oxidative stress in *A1cf* $^{+/Tg}$ mice and found that total glutathione levels were significantly elevated in *A1cf* $^{+/Tg}$ liver (Supplemental Figure 7A), with no change reduced or oxidized glutathione and no change in mRNAs involved in glutathione synthesis (Supplemental Figure 7A). We also found no evidence for increased endoplasmic reticulum stress as evidenced by mRNA abundance of *Chop*, *Ire1a*, *Xbp1*, *Grp78* and *Atf4* (Supplemental Figure 7B).

To further examine the range of potential A1CF mRNA targets, we undertook RNA-CLIP Seq (28) on isolated hepatocytes from *A1cf* $^{+/Tg}$ mice (Supplemental Figure 7C) and identified 245

RNAs that co-purified with FLAG-tagged A1CF (here designated direct A1CF targets). Overlapping these direct A1CF RNA targets with mRNAs that were significantly differentially expressed in our RNA-Seq studies, we identified 4 A1CF RNA targets (*Sox4*, *Sparcl1*, *Smad9* and *Dlgap1*) (Figure 9). Q-PCR revealed 1.5-fold and 2-fold up-regulation of *Sox4* and *Sparcl1* mRNAs respectively, with 2-fold and 10-fold down-regulation of *Smad9* and *Dlgap1* mRNAs respectively (Figure 9). Those mRNAs revealed a trend towards the inverse patterns in *A1cf* $^{-/-}$ liver (Supplemental Figure 7D). *SOX4* overexpression in liver was shown to stabilize β-CATENIN, increase cell proliferation, promoting steatosis and HCC progression (29-32), while *SPARCL1* overexpression was correlated with tumor angiogenesis in HCC (33, 34). Since SMAD9 inhibits Bone Morphogenetic Protein (BMP) signaling (34) we asked if the decreased expression of *Smad9* in *A1cf* $^{+/Tg}$ liver was accompanied by changes in *Bmp7* mRNA. Q-PCR revealed a 2-fold increase in *A1cf* $^{+/Tg}$ liver (Supplemental Figure 7E), findings consistent with the fibrogenic phenotype observed in *A1cf* $^{+/Tg}$ mice. Those findings, taken together, support the notion that mRNAs identified through RNA-CLIP are likely direct A1CF targets with a plausible role in the phenotypes observed. Among the differentially expressed RNAs, we also observed increased abundance of several organogenic mRNAs (*Sox9*, *Gpc1*, *Tmprss4*) in *A1cf* $^{+/Tg}$ mice (Supplemental Figure 7F). Among the features of interest in those mRNAs, the presence of an AU-rich 3'UTR in *Sox9* mRNA, led us to ask if *Sox9* mRNA could represent a target for A1CF since earlier work showed that A1CF is an AU-rich RNA binding protein (11). Here we show that *Sox9* RNA was immunoprecipitable from liver extracts and demonstrated a shift into actively translating polysomal RNA fractions (Supplemental Figure 7F).

We also undertook transcriptome profiling in isolated hepatocytes, revealing 391 upregulated and 574 downregulated RNAs (Figure 10A). *Cd36* mRNA was ~4-fold upregulated (compare Figure 10A to Figure 3B for whole liver), again supporting the conclusion that hepatocyte *Cd36* expression is regulated in response to A1CF overexpression. We aligned A1CF RNA targets

identified by RNA-CLIP with differentially expressed RNAs in *A1cf* $^{+/Tg}$ hepatocytes and validated differential expression of 2 mRNAs, *Dram1* and *Phlda2*, which showed 2-2.5 fold higher levels in *A1cf* $^{+/Tg}$ hepatocytes (Figure 10B). Gene ontology analysis revealed enrichment of pathways related to inflammatory response, supporting the phenotype observed in *A1cf* $^{+/Tg}$ liver (Figure 11A) and consistent with a predicted increase in proinflammatory cytokine and chemokine production (35), including *IL19*, *Cxcl14* and *TNF*α mRNAs, which were 5-12 fold upregulated in *A1cf* $^{+/Tg}$ hepatocytes (Figure 11A). We also analyzed markers of inflammation in whole liver from *A1cf* $^{+/Tg}$ mice and observed a significant increase in mRNAs encoding proinflammatory chemokines including CCR2 and CXCL14 which likely contribute to inflammation as shown by elevated expression of *Ly6c* and *Tnf*α mRNAs (Figure 11A). In addition, we examined expression of mRNAs encoding tumor suppressor genes (TSG) and oncogenes (Figure 11B), revealing 49 TSG mRNAs and 2 oncogene mRNAs among the differentially expressed genes from the RNA-Seq analysis. Of the 49 TSG mRNAs, 26 clustered in functional categories including transcriptional regulation, cell cycle and protein phosphorylation, supporting the phenotype observed in *A1cf* $^{+/Tg}$. Among the 26 TSG mRNAs, 7 showed more than 3-fold alteration by RNA-Seq of which 4 TSG mRNAs (*Pbrm1*, *Rb1, Sall2* and *Cdh24*) validated by quantitative PCR, were significantly downregulated (Figure 11B), while 2 oncogenes (*Jak3*, *Klf4*) exhibited increased mRNA abundance in *A1cf* $^{+/Tg}$ liver (Figure 11B).

Whole liver transcriptome analysis in aged *A1cf* $^{+/Tg}$ liver.

The data presented above suggest that A1CF overexpression promotes steatosis, hepatocyte proliferation as well as activating inflammatory and fibrogenic pathways in both whole liver and isolated hepatocytes from young mice. In order to understand the tumorigenic pathways in older mice, we next profiled mRNAs in aged (12 month) *A1cf* $^{+/Tg}$ liver, which revealed 1505 differentially expressed RNAs (Figure 12A). Gene Ontology and KEGG analysis revealed

enrichment in genes related to extracellular matrix organization (Figure 12B). We aligned differentially expressed RNAs with RNA-CLIP A1CF targets and identified 6 A1CF RNA targets: 4 with increased abundance (*Spag5*, *Phlda2*, *Abcc12* and *Cdh1*) and 2 (*Dmrta1* and *Irx1*) with decreased abundance in *A1cf* $^{+/Tg}$ livers, (Figure 12C and 13). We attempted to assign a definitive role for A1CF in the regulation of these RNAs by examining hepatic mRNA expression in aged *A1cf* $^{-/-}$ mice, where we reasoned that mRNAs that were increased in *A1cf* $^{+/Tg}$ livers would be correspondingly reduced in the livers of *A1cf* $^{-/-}$ mice. Of the 6 RNAs identified above, only E cadherin 1 (*Cdh1*) met the criteria for a gain-of-function/loss-of-function effect (ie upregulated in *A1cf* $^{+/Tg}$ and downregulated in age-matched *A1cf* $^{-/-}$ liver (Figure 13). *Abcc12* mRNA was 5-fold upregulated in *A1cf* $^{+/Tg}$ liver, recapitulating findings showing increased expression in breast cancer (36) and loss of A1CF attenuated this increase in mRNA expression (Figure 13). The remaining 4 RNAs (*Spag5*, *Phlda2*, *Dmrta1*, *Irx1*) were unchanged in WT and *A1cf* $^{-/-}$ liver (Figure 13 and Supplemental Figure 8). We examined features of the 12 mRNAs identified through RNA-CLIP Seq as possible A1CF targets, focusing on the 3' untranslated region (Supplemental Table S1). The majority of those mRNAs (11/12) were enriched in AU sequences, containing at least one AUUUA motif or stretches (5 or 6 repeats) of poly (U) elements (Supplemental Table S1). Those sequence and context preferences are consistent with findings from earlier studies (37). Only one mRNA (*Abcc12*) contained none of those features and contained <50% AU content (Supplemental Table S1).

A role for A1CF in human hepatocellular cancer:

Genome-wide association studies implicate *A1CF* in regulating hepatic lipid metabolism and plasma TG levels (15). Because genetic pathways in hepatic lipid metabolism modulate HCC risk in patients with NAFLD (38), we took advantage of The Cancer Genome Atlas (TCGA) and observed that 6 A1CF RNA targets (*Spag5*, *Abcc12*, *Phlda2*, *Cdh1*, *Dmrta1*, *Irx1*, Supplemental Figure 9A) that were differentially expressed in 12-month old *A1cf* $^{+/Tg}$ mouse liver were also

associated with aberrant expression of A1CF in human HCC. Of the 6 RNAs, *Spag5* and *Cdh1* mRNAs showed a significant positive co-occurrence with A1CF (Supplemental Figure 9A). Alterations in A1CF were observed in 9% of 360 patients with HCC, including increased gene copy number and increased mRNA expression in a subset as well as reduced A1CF expression in another subset, the latter reflecting either decreased mRNA or mutational alteration (Supplemental Figure 9A). Those findings hint at the possibility that A1CF expression might be altered in patients with HCC.

To resolve that possibility, we examined immunohistochemical expression of A1CF in normal control subjects, cirrhotic patients and in patients with HCC. We observed homogeneous nuclear A1CF staining in control subjects (Figure 14A, upper panel), with heterogeneous staining in cirrhotic nodules as well as in HCC with increased nuclear expression at the edge of the invasive front of the tumor (Arrowheads, Figure 14A, lower panel). We also performed immunohistochemical analysis of A1CF expression in a tissue microarray of human HCC samples generated at Mayo Clinic, Rochester, MN (clinical data included in Supplemental table S2). We categorized A1CF staining into four groups based on average sample pixel intensity per high power field, in both tumor and uninvolved tissue (Figure 14B and Table 3). High level of A1CF staining correlated with advanced (F3/4) fibrosis in both uninvolved and tumor tissue from the entire cohort (Figure 14C) and was also correlated with higher levels of alfa fetoprotein levels (Figure 14D). We used multivariable Cox proportional hazard modeling to show that A1CF staining intensity in the uninvolved tissue was predictive of overall survival, with worst survival associated with highest levels of A1CF expression. This implied prognostic role of increased A1CF staining intensity was independent of TNM stage, tumor number, and other putative prognostic factors included in the final model (Supplemental table S3). Among a subgroup of 19 HCC patients where NAFLD was a potential underlying etiology (Methods and Supplemental table S4), the adverse prognostic role of increased A1CF staining intensity was

further substantiated with a progressive decrease in overall survival apparent in patients with increasing levels of A1CF expression (Figure 14E). Furthermore, using proportional hazard modeling, we found that A1CF expression remained predictive of survival after adjusting for recurrence and time to first recurrence in the subgroup with NAFLD (Supplemental table S5). We also confirmed a significant, independent association of mRNA expression of *A1CF* with *SPAG5* and with *CDH1* in a second cohort of patient samples (Supplemental Table S6) of normal and cirrhotic liver (Supplemental Figure 9B), suggesting that the associations demonstrated in mice overexpressing *A1cf* may also be relevant to conditions (ie cirrhosis) that predispose to HCC in humans.

Discussion

Here we show that transgenic overexpression of the RNA binding protein A1CF in mouse liver produces a gain-of-function phenotype that includes steatosis, increased proliferation, inflammation fibrosis and spontaneous tumorigenesis. As an overarching model (Figure 15), we show that A1CF overexpression alters hepatic APOB secretion and shifts VLDL production into smaller particles which, along with upregulation of mRNAs including lipogenic genes and *Cd36*, promotes the development of hepatic steatosis. In addition, upregulation of mRNAs involved in oxidative stress, inflammation and extracellular matrix organization in *A1cf* $^{+/Tg}$ mice promotes the development of hepatic fibrosis. The convergence of these steatotic and fibrogenic pathways, together with upregulation of proliferative and organogenic mRNAs and decreased expression of tumor suppressor mRNAs, promotes spontaneous tumorigenesis and HCC (Figure 15). Several elements of our findings and this proposed model merit further discussion.

A1CF is a widely expressed RNA binding protein identified in connection with *ApoB* RNA binding and assembly of a functional C-to-U RNA editing complex with APOBEC1 (9, 10). However, *A1cf* deletion produced no effect on *ApoB* RNA editing (12) and variably impacted C-to-U RNA editing of other mRNAs (13). More recently, genome-wide association studies implicated variants in *A1CF* with specific metabolic traits, including regulation of plasma triglyceride levels (15, 39). Accordingly, among the primary objectives of this study was to examine the impact of gain- and loss-of-function of A1cf alleles on hepatic RNAs and in particular the impact on VLDL assembly and secretion. Findings demonstrating CRISPR-mediated *A1CF* deletion in human hepatoma cells greatly decreased APOB secretion (15), led us to predict that VLDL production and fasting plasma triglyceride levels would be correspondingly reduced in *A1cf* $^{+/Tg}$ mice and elevated in *A1cf* $^{-/-}$ mice. However, those predictions were only partially confirmed. We found a modest decrease in APOB secretion and

a shift to smaller VLDL particles in *A1cf* $^{+/Tg}$ mice. However, there were no alterations in hepatic triglyceride or VLDL secretion, or in APOB production in *A1cf* $^{-/-}$ mice and only a subtle (~30%) decrease in APOB secretion from two independent *A1CF* null HepG2 cells. Our transcriptomic surveys further revealed a panel of hepatic mRNAs whose expression was upregulated in *A1cf* $^{+/Tg}$ mice, including *Cidea*, *Mogat1*, *Mogat2* and *Cd36* via mechanisms that include shifts into actively translating polysome fractions and increased protein expression. A function for A1CF in transporting mRNAs towards actively translating polysomes is consistent with its known nuclear:cytoplasmic shuttling activity in cell culture models (14, 40) and with its dynamic pattern of altered distribution under metabolic stress (23).

We further observed that aged *A1cf* $^{+/Tg}$ mice developed advanced fibrosis and that male mice developed spontaneous liver tumors at high penetrance, even while consuming a chow diet. The tumorigenic phenotype was accelerated by feeding male mice a high fat, high fructose diet and those mice exhibited hepatic STAT-3 activation along with downstream effects including upregulation of *Hif1*α mRNA, consistent with prior studies linking experimental obesity-associated NASH to advanced features including development of HCC (41). Those tumors exhibited features associated with human HCC, including immunohistochemical staining for GPC3, HSP70, enhanced β-CATENIN expression and increased expression of CYCLIN D1. Certain features of the temporal progression from steatosis to fibrosis raise the question of whether the development of HCC in *A1cf* $^{+/Tg}$ mice occurs as a consequence of—or independently from—fibrogenic and inflammatory signaling? The demonstration that *A1cf* $^{+/Tg}$ mice fed high fat, high fructose diets exhibit enhanced steatosis and inflammatory signaling (augmented STAT3 activation, Figure 7 A, B) along with dysplastic nodules, suggests that the progressive development of HCC is likely driven by steatotic injury and fibrogenic signaling. On the other hand, our findings that WT and *A1cf* $^{-/-}$ mice also develop steatosis, fibrosis and

inflammation when fed high fat, high fructose diets yet mice of neither genotype develop tumors at 6 months (in contrast to *A1cf* $^{+/Tg}$ mice) suggests that the presence of steatosis and fibrosis alone are insufficient to promote HCC.

As a step towards identifying relevant signaling pathways, we undertook RNA-Seq from livers of *A1cf* $^{+/Tg}$ mice at various ages and aligned some of the differentially expressed mRNAs with RNA-CLIP Seq from isolated hepatocytes. We identified 12 mRNAs through RNA-CLIP Seq and discovered several shared sequence motifs within the 3' untranslated region of those mRNAs, including the overall AU content, the presence and multiplicity of AUUUA motifs and the presence and multiplicity of poly (U) stretches. The preference for AU and poly U motifs is consistent with recent work (37) and those preferences are shared by other RNA binding proteins, including RBM47 and members of the hnRNP family (hnRNPH1/2), both of which have been shown to interact with A1CF in posttranscriptional regulation (13, 23). Among the RNA-CLIP targets, *Cdh1* and *Spag5* both have plausible roles in the pathogenesis of HCC. Germline or somatic (loss-of-function) mutations in *CDH1* are well recognized in a range of cancers including HCC (42, 43), but *CDH1* mRNA has also been shown to be upregulated in 40% of patients with HCC (44), with findings demonstrating selective nuclear retention of *CDH1* mRNA in some patients (45). Those latter findings raise the question of whether nucleo-cytoplasmic shuttling activity of A1CF (40) plays a role in compartmentalizing specific cargo RNAs in tumorigenesis. Another A1CF target, *SPAG5*, was upregulated (mRNA and protein) in HCC and associated with poor survival (46). Furthermore, expression of both *CDH1* and *SPAG5* RNA was highly correlated with *A1CF* RNA in patients with cirrhosis (Supplemental Figure 9B). Yet another A1CF target, *Sox9* mRNA, which was immunoprecipitated from hepatocytes from *A1cf* $^{+/Tg}$ mice, was identified as a hepatic stem cell marker in HCC with *SOX9* overexpression in patients correlating with reduced overall survival (47).

As far as other RNA targets, A1CF likely interacts with RBM47 in the context of C-to-U RNA editing of *ApoB* mRNA and modifies editing activity of the RNA deaminase APOBEC1 on a variety of substrates in mouse liver and intestine (13). A1CF competes with hnRNPH1/2 by binding at the 5' splice site of exon 3C in ketohexokinase mRNA and regulates alternative splicing (23). However, we failed to observe spontaneous liver tumors in aged, male *A1cf* $^{-/-}$ mice where this alternative splicing event would be predicted to increase expression of ketohexokinase mRNA with the A-isoform, a shift in isoform distribution that was shown in other work to promote growth of hepatoma cells in nude mice (24). An additional caveat is warranted in the interpretation of the temporal shifts in hepatic mRNA expression noted in *A1cf* $^{+/Tg}$ mice since those changes likely reflect both altered cellular expression and cellular composition. Resolution of these possibilities will require study of the cellular composition and transcriptomic profiles at critical developmental stages.

While we confirmed the same pattern of nuclear A1CF staining in human hepatocytes and mouse liver (48), we also observed heterogeneity in A1CF expression in cirrhosis and HCC with variability in regenerating nodules and tumors. We found increased levels of staining were associated with more advanced stages of fibrosis as well as other parameters of advanced liver disease (Child-Pugh score and MELD score) (Supplemental table S2). In HCC patients where NAFLD was an underlying etiology, high levels of A1CF staining were predictive of reduced overall survival. Those observations must be interpreted with caution however. First, this cohort of HCC contained only 19 subjects (14%) with NAFLD and our study was not powered to draw conclusions regarding specific HCC etiology. However, the overall prevalence of NAFLD underlying HCC is very similar to previous retrospective cohorts reported from Mayo Clinic (49). Secondly, while fibrosis stage is an important predictor of all-cause mortality in NAFLD patients (50), it is unclear whether A1CF expression is associated with compensated cirrhosis and/or bridging fibrosis. This reservation is relevant also to our observations that A1CF staining is

within hepatocytes, suggesting the possibility that steatotic hepatocytes release factors that promote fibrogenic and/or inflammatory signaling (51). Thirdly, our conclusions regarding A1CF expression in those samples reflect immunohistochemical staining intensity, which is at best semi-quantitative. Future studies will be required to obtain a more granular understanding of A1CF protein distribution and expression in relation to the candidate mRNAs implicated and to examine the role of RNA trafficking, polysome distribution and translation of those candidate target genes.

METHODS.

Animals: *A1cf* $^{-/-}$ and *Apobec1* $^{-/-}$ mice were on a background of C57BL/6NJ or C57BL/6J, respectively, (13, 52). For high fat diet studies mice were fed a high trans-fat, fructose (TFF) diet (TD.06303, Envigo, Indianapolis, IN, USA) for 6 months. Unless noted otherwise, mice were fasted 4 h and injected with 100 mg/kg of bromodeoxyuridine (Sigma, St Louis, MO, USA) 2 h before study. Littermate controls were used in all experiments.

Generation of A1cf transgenic mice: The FLAG-A1cf transgene was generated by amplification of A1cf from human cDNA using a 5' primer containing Flag sequence and a KpnI site and a 3' primer containing an XhoI site and cloned into the pLiv7 vector (53). Of five founders, two were selected with comparable levels (~2-3-fold) of transgene expression for the baseline characterization and original description of spontaneous tumorigenesis.

Liver and serum biochemical assessments: Serum levels of alanine aminotransferase (ALT) and aspartate aminotransferase (AST) were measured with kits (TECO DIAGNOSTICS, Anaheim, CA, USA). Serum and hepatic triglycerides (TG), cholesterol and NEFA levels were measured using kits (Fuji Film Wako Diagnostics, Mountain View, CA, USA). Serum was fractionated on tandem Superose 6 columns (Pharmacia FPLC). Liver glutathione was evaluated following manufacturer's protocol (Cayman Chemical, Ann Arbor, MI, USA).

VLDL secretion: Following a 4 or 16h fast mice were weighed, injected with Pluronic F-127 (1 mg/g) (Invitrogen) and serum triglyceride determined from blood collected 1, 2 and 4h after injection.

Electron microscopy: Pooled serum from 2 to 4 mice was collected after Pluronic F-127 injection and VLDL particles separated by ultracentrifugation for negative staining electron microscopy.

Histology and Immunohistochemistry: For mouse studies, BrdU-positive hepatocytes were quantitated in each section. Eight to 10 fields per section, each section containing 4 to 6 pieces of liver from multiple lobes, were analyzed. Fibrosis was assessed by Sirius red-staining. Using Nuance multispectral imaging software a spectral library was created to analyze a complete experimental group. Liver sections (4 μm) were stained with anti-A1CF, anti-FLAG, anti-CIDEA, anti-β-CATENIN, anti-HSP70, anti-GPC3, anti-p62 and anti-CYCLIN D1. Dilutions and origins of each antibody are given in Supplemental Table S7. Histological survey was performed by a pathologist blinded to the experimental groups. Liver nodules were counted and classified into dysplastic nodules and HCC. The background liver was evaluated for the presence of steatosis, inflammation, ballooning and anisonucleosis. For human samples, TMA slides were scanned using Nuance FX multispectral imaging system (CRi, Cambridge Research & Instrumentation, Woburn, MA) and a Nuance 2.10 software. Images were acquired at 20 nm wavelength intervals and combined into one image. A spectral library was created and served as reference with individual fluorescent signals corresponding to total A1CF, nuclear A1CF, counterstain (haematoxylin) and autofluorescence. Autofluorescence was substracted from the spectral reference. Two 20x magnification fields per sample were randomly analyzed. The emission spectra for total and nuclear A1CF were acquired and saved as image cube that contains both individual signal components that were then unmixed and analyzed separately. The intensity of staining was defined by pixels evaluated in the analyzed area, including the entire field for total A1CF staining and all nuclei for nuclear staining. Total pixel values for total and nuclear A1CF represent the mean of two measurements per sample. Stained area was expressed as a percentage of total area. Unstained samples were evaluated using the same parameters used to create the spectral reference (fluorescent signals for both total and nuclear A1CF, counterstain and autofluorescence). These samples showed only counterstaining background. Samples were considered positively stained when the total pixel value was above counterstain background.

Studies in primary hepatocytes: Livers were perfused, digested with 0.05% collagenase (Type IV, C5138, Sigma) and hepatocytes plated on collagen-coated dishes overnight. APOB synthesis and secretion was studied as described (54), with ^{35}S-methionine pulsed for 30 min and chased for 0, 2 and 4 h. Aliquots of cell lysate and medium were immunoprecipitated with APOB IgG and separated by 4-15% gradient SDS-PAGE. The data was normalized to total TCA precipitable radioactivity. CRSPR targeted HepG2 cells were generated as described (17).

RNA extraction and RNA-Sequencing: For each genotype and condition, 3 pools were prepared, each containing RNAs from 3-4 separate mice, for a total of 10 mg RNA per final pool. Pools were subjected to oligo(dT) selection and cDNA library preparation and whole transcriptome sequencing by Illumina HiSeq2000 as described (55).

Gene expression analysis by quantitative PCR: Total RNA was treated with DNAse and subjected to cDNA synthesis using High Capacity cDNA Reverse Transcription kit (Applied biosystems). Quantitative PCR was performed in triplicate. RNA levels were expressed as fold changes after normalization to glyceraldehyde-3-phosphate dehydrogenase (*Gapdh*) RNA. Sequences of primers used for quantitative PCR are listed in Supplemental Table S8.

Polysome isolation: Livers were washed in ice-cold phosphate buffered saline supplemented with 0.1 mg/ml cycloheximide (Sigma, St Louis, MO, USA) and minced in lysis buffer (25 mM Tris-HCl pH 7.5, 250 mM NaCl, 5 mM $MgCl_2$, 0.5 mM PMSF, 0.2 mg/ml heparin (Sigma), 5 mM dithiothreitol, 20 U/ml RNAsin, 0.1 mg/ml cycloheximide, 1% Triton X-100, 1X protease inhibitor). Homogenized minced livers were resolved through a 10-50% sucrose gradient at 40,000 rpm for 2.5 h at 4 °C using a SWT41i rotor (Beckman Brea, CA, USA). Fractions (0.9 ml) were collected

and 260 nm absorbance monitored by spectrophotometry. RNA from each fraction was used for quantitative PCR.

Protein extraction and Western blot analysis: 50 µg protein were resolved by SDS-PAGE and transferred to PVDF membrane. In all analyses, equal loading was verified using anti- ACTIN or anti-GAPDH antibody. Antibodies and conditions used for western blot are listed in Supplemental Table S7.

A1CF-RNA Co-immunoprecipitation: A1CF-RNA co-immunoprecipitation was performed as described (11). Freshly harvested, minced livers were exposed to 300 mJ/cm^2 UV irradiation in a Stratalinker 1800 (Stratagene), collected in 1X PBS, and resuspended into PLB buffer (10 mM HEPES, pH 8, 100 mM KCl, 5 mm $MgCl_2$, 10 mM ribonucleoside vanadyl complexes (Sigma), 0.5% Nonidet P-40, 1 mM dithiothreitol, 0.2 mM phenylmethylsulfonyl fluoride and protease inhibitors). Cleared lysates were incubated with 0.1 ml of pre-swollen magnetic Dynabeads protein A beads (Invitrogen). Aliquots were extracted with TRIzol as input RNA. The remainder was incubated overnight, with either protein A coupled to anti-A1CF (25 µg), or rabbit IgG in NT2 buffer (50 mM Tris, pH 7.4, 150 mM NaCl, 1 mM $MgCl_2$, 0.05% Nonidet P-40) supplemented with 200 units RNase inhibitor (Invitrogen), 2% ribonucleoside vanadyl complexes, 1 mM dithiothreitol, 150 mM EDTA. The beads were washed twice in Buffer A (1× PBS (no Mg^{2+}, no Ca^{2+}), 0.1% SDS, 0.5% deoxycholate, 0.5% Nonidet P-40), twice in Buffer B (5× PBS (no Mg^{2+}, no Ca^{2+}), 0.1% SDS, 0.5% deoxycholate, 0.5% Nonidet P-40), and twice in Buffer C (50 mM Tris, pH 7.4,10 mM $MgCl_2$, 0.5% Nonidet P-40). Beads were incubated 30 min at 55 °C with 30 µg of proteinase K (Sigma) and 0.1% SDS in 1X NT2 buffer supplemented with 80 units of RNase OUT (Promega). The phenol/chloroform-extracted RNA was used for cDNA synthesis followed by PCR using Sox9 – specific primers: Fwd825 5'-GAAGAGACCCTTCGTGGAGGAGGCGG-3' Rev1040 5'-

TGCACCTCACTCATGCCGGAGGAGG-3'. PCR products from A1CF-specific IP were gel-purified and sequenced.

RNA CLIP-Seq was performed as described (28). Primary hepatocytes (10^8) from 12 week-old *A1cf* $^{+/Tg}$ mice seeded on 10 mm collagen-coated plates, were exposed to 400mJ/cm^2 of 254 nm UV light in a Stratalinker 2400 (Stratagene). Hepatocytes were scraped in 1ml Lysis buffer containing 50 mM HEPES pH 7.5, 150 mM KCL, 2 mM EDTA, 1 mM NaF, 0.5% (v/v) NP40, 1 mM DTT, 1x protease inhibitors, 2 mM Na_3VO_4, 5 mM Sodium Pyrophosphate and RNAsin (Promega), incubated on ice and frozen at -80 °C. Cells were homogenized and cleared lysates were treated with RQ1 DNAse (Promega) 5 min at 37 °C followed by 15 min incubation at room temperature with RNAse T1 (Fermentas). A1CF-RNA complexes were immunoprecipitated and treated on-beads with RNAse-T1, ligated with RNA adapters (RL5a-TYE705 and RL3-biotin), resolved on SDS-PAGE and transferred to nitrocellulose. The RNP complexes were excised and treated with Proteinase K (Thermo Scientific). Phenol/chloroform-purified RNA was subjected to cDNA synthesis using DP3 primer, followed by PCR using DP5a and DP3 primers. PCR conditions were as followed: 94 °C 2 min, 40 cycles at 94 °C 30 sec, 58 °C 30 sec, 68 °C 30 sec, 68 °C 10 min. PCR products were gel-purified and subjected to a second round of amplification using DSFP5a and indexed DSFP3 primer (RPIX-D3) (one per template) with the following conditions: 94 °C 2 min, 35 cycles at 94 °C 30 sec, 62 °C 45 sec, 68 °C 45 sec, 68 °C 10 min. Final PCR products were gel purified and submitted for High throughput sequencing using primer SSP1. Primer sequences are as followed:

RL5a-TYE705: 5'-AGGGAGGACGAUGCGG-3'; **RL3-biotin**: 5'-GGCGACCUUCACUGACUGUG-3'; **DP5a**: 5'-AGGGAGGACGATGCGG-3'; **DP3**: 5'-CCGCTGGAAGTGACTGACAC-3'; **DSFP5a**: 5'-AATGATACGGCGACCACCGACTATGGATACTTAGTCAGGGAGGACGATGCGG-3'; **RPIX1-DP3**: 5'-CAAGCAGAAGACGGCATACGAGAT**CGTGAT**GTG-

ACTGGAGTTCCTTGGCACCCGAGAATTCCACCGCTGGAAGTGACTGACAC-3'. The underlined 6 nucleotide-sequence in bold represents the index. Each index is as followed: **RPIX2-DP3**: ACATCG, **RPIX3-DP3**: GCCTAA, **RPIX4-DP3**: TGGTCA, **RPIX5-DP3**: CACTGT, **RPIX6-DP3**: ATTGGC, **RPIX7-DP3**: GATCTG, **RPIX8-DP3**: TCAAGT, **RPIX9-DP3**: CTGATC. **SSP1**: 5'-CTATGGATACTTAGTCAGGGAGGACGATGCGG-3'.

Bioinformatic analysis: Microarray data was processed using the R/Bioconductor package Limma (51). Background correction was performed using the normexp + offset method (56). The loess and scale methods (57) were used for normalization within and between arrays, respectively. RNA-Seq reads were aligned to the Ensembl release 76 primary assembly with STAR version 2.5.1a (58). Unsupervised hierarchical clustering of samples was performed with Cluster3 (59) and heat maps were generated with Java TreeView (60). Gene counts were derived from the number of uniquely aligned unambiguous reads by Subread:featureCount version 1.4.6-p5 (61). Isoform expression of known Ensembl transcripts was estimated with Salmon version 0.8.2 (62). All gene counts were imported into the R/Bioconductor package EdgeR (63) and TMM normalization size factors were calculated to adjust for differences in library size. The TMM size factors and the matrix of counts were imported into the R/Bioconductor package Limma (64). Weighted likelihoods based on the observed mean-variance relationship of every gene and sample was calculated for all samples with the voomWithQualityWeights (65). Differential expression analysis was performed to analyze for differences between conditions and the results were filtered only for the genes with Benjamini-Hochberg false-discovery rate adjusted p-values less than or equal to 0.05. The Database for Annotation, Visualization, and Integrated Discovery (DAVID) tool (66, 67) was used to identify enrichment for functional pathways within differentially expressed gene sets.

Data availability: The RNA-Seq and RNA-CLIP data discussed in this publication have been deposited in NCBI's Gene Expression Omnibus and are accessible through GEO Series accession number GSE157233 (https://www.ncbi.nlm.nih.gov/geo/query/acc.cg?acc=GSE157233). The RNA array data are accessible through GEO Series accession number GSE157516. (https://www.ncbi.nlm.nih.gov/geo/query/acc.cgi?acc=GSE157516).

Statistical analysis: Data are mean ± SE for the indicated sample number. Statistical significance was set at a *P* value < 0.05. Data were analyzed using GraphPad Prism 7.02 (GraphPad Software, Inc. La Jolla, CA, USA) by unpaired t-test or Mann-Whitney U test. For multigroup comparisons, statistical differences were performed by one-way ANOVA and Tukey's multiple comparison post-hoc test.

Statistical analyses on the clinical samples were performed using the average A1CF expression of paired samples (pixel count per high power field) per tissue type. Unpaired t-test or one-way ANOVA were used to compare A1CF expression of tumor or uninvolved tissue across subgroups of HCC patients categorized based on different clinical and paraclinical parameters. For survival analysis, we used Kaplan-Meier curves to estimate overall survival patterns in patients with different levels of A1CF expression. We also used Cox proportional hazard modeling to adjust prognostic role of A1CF expression in HCC patients for other putative prognostic factors. First, simple Cox models were used to identify factors associated with overall survival of patients. Next, we fit the preliminary multivariable model based on A1CF and other candidate factors identified from previous step and used backward elimination method to reach the final multivariable Cox proportional hazard model. Prognostic factors with significant hazard ratios or major contribution to fitness of the model were retained in the final Cox model. We also investigated the prognostic role of tissue A1CF expression in a subset of HCC patients with NAFLD (N=17/19, Supplemental Table S4). The association between A1CF expression and overall survival was also adjusted for recurrence and time to the first recurrence in this

subgroup. Statistical analysis of clinical data was conducted using Stata statistical software version SE 11.2 (StataCorp LP, College Station, TX).

Study approval: All animal experiments were conducted in accordance with the institutional guidelines of animal care and use committee of Washington University School of Medicine (IACUC #20180266, 20190028).

Studies with human subjects: Deidentified human liver tissue blocks were obtained from the Department of Pathology at Washington University School of Medicine. For the evaluation of HCC samples, a total of 137 patients were analyzed from a patient cohort at Mayo Clinic, Rochester, MN, which were collected with approval from the Mayo Clinic Institutional Review board (IRB # 16-003945). A tissue microarray was constructed using two uninvolved and two tumor tissue samples per patient, which were analyzed for A1CF expression by immunohistochemistry. Available clinical and laboratory data are presented in Supplemental Table S2. Patients were followed for an average of 3.7 years after diagnosis. Patients were classified as having NAFLD as an underlying component of HCC if (1) confirmed by history and pathologic examination; (2) among patients with BMI >30 (>25 for Asians) where there was no other identified etiology (viral hepatitis, alcohol etc). A1CF expression was defined as total pixels per high power field and categorized as follows: Category 1 (< $12E^4$ pixels), category 2 ($12\ E^4$-$23\ E^4$ pixels), category 3 ($23\ E^4$-$32\ E^4$ pixels), category 4 (>$32\ E^4$ pixels). A second cohort of patient samples were obtained from cirrhotic and normal liver tissue in patients undergoing surgical resection at Queen Mary Hospital, Hong Kong. Sample collection was approved by the Institutional Review Board of the University of Hong Kong/Hospital Authority Hong Kong West Cluster (UW 09-185) and informed consent was obtained from patients prior to tissue collection and analysis. Demographic data for these subjects is shown in Supplemental Table S6.

Author contributions:

Study design and approach: VB, NOD

Experimental methodology, animal and cell studies: VB, JDR, EMQ, YX

Pathology and immunohistochemical analysis: VB, IN, EMB, JCM, IN, YH, LRR

Bioinformatics analysis: JDR, VB, JHN, SS, BBM, JCM, DCR

Data interpretation: VB, JDR, JHN, JCM, DCR, IN, YH, LRR, NOD

Manuscript preparation and final review: All authors

Acknowledgments:

This work was supported by grants (DK112378 to DCR, NOD; DK 119437 to NOD; Washington University Digestive Disease Research Core Center P30 DK 52574 (AITAC and Biobank Cores) to NOD, DCR, JCM); grant RGC TRS T12-704/16-R to ION; grants DK 106382, CA 230282 (DCR); P50 CA210964 (Mayo Clinic Hepatobiliary SPORE) from the National Cancer Institute (LRR); R01DK105129 and R01DK094989 (JCM).

REFERENCES

1. Rinella M, Charlton M. The globalization of nonalcoholic fatty liver disease: Prevalence and impact on world health. Hepatology 2016;64:19-22.
2. Forner A, Llovet JM, Bruix J. Hepatocellular carcinoma. Lancet 2012;379:1245-1255.
3. Adams LA, Anstee QM, Tilg H, Targher G. Non-alcoholic fatty liver disease and its relationship with cardiovascular disease and other extrahepatic diseases. Gut 2017;66:1138-1153.
4. Sookoian S, Pirola CJ, Valenti L, Davidson NO. Genetic Pathways in Nonalcoholic Fatty Liver Disease: Insights From Systems Biology. Hepatology 2020;72:330-346.
5. Pirola CJ, Sookoian S. The dual and opposite role of the TM6SF2-rs58542926 variant in protecting against cardiovascular disease and conferring risk for nonalcoholic fatty liver: A meta-analysis. Hepatology 2015;62:1742-1756.
6. Reyes-Soffer G, Moon B, Hernandez-Ono A, Dionizovik-Dimanovski M, Jimenez J, Obunike J, Thomas T, et al. Complex effects of inhibiting hepatic apolipoprotein B100 synthesis in humans. Sci Transl Med 2016;8:323ra312.
7. Panta R, Dahal K, Kunwar S. Efficacy and safety of mipomersen in treatment of dyslipidemia: a meta-analysis of randomized controlled trials. J Clin Lipidol 2015;9:217-225.
8. Cuchel M, Meagher EA, du Toit Theron H, Blom DJ, Marais AD, Hegele RA, Averna MR, et al. Efficacy and safety of a microsomal triglyceride transfer protein inhibitor in patients with homozygous familial hypercholesterolaemia: a single-arm, open-label, phase 3 study. Lancet 2013;381:40-46.
9. Lellek H, Kirsten R, Diehl I, Apostel F, Buck F, Greeve J. Purification and molecular cloning of a novel essential component of the apolipoprotein B mRNA editing enzyme-complex. J Biol Chem 2000;275:19848-19856.
10. Mehta A, Kinter MT, Sherman NE, Driscoll DM. Molecular cloning of apobec-1 complementation factor, a novel RNA-binding protein involved in the editing of apolipoprotein B mRNA. Mol Cell Biol 2000;20:1846-1854.
11. Blanc V, Sessa KJ, Kennedy S, Luo J, Davidson NO. Apobec-1 complementation factor modulates liver regeneration by post-transcriptional regulation of interleukin-6 mRNA stability. J Biol Chem 2010;285:19184-19192.
12. Snyder EM, McCarty C, Mehalow A, Svenson KL, Murray SA, Korstanje R, Braun RE. APOBEC1 complementation factor (A1CF) is dispensable for C-to-U RNA editing in vivo. RNA 2017;23:457-465.
13. Blanc V, Xie Y, Kennedy S, Riordan JD, Rubin DC, Madison BB, Mills JC, et al. Apobec1 complementation factor (A1CF) and RBM47 interact in tissue-specific regulation of C to U RNA editing in mouse intestine and liver. RNA 2019;25:70-81.
14. Galloway CA, Ashton J, Sparks JD, Mooney RA, Smith HC. Metabolic regulation of APOBEC-1 complementation factor trafficking in mouse models of obesity and its positive correlation with the expression of ApoB protein in hepatocytes. Biochim Biophys Acta 2010;1802:976-985.
15. Liu DJ, Peloso GM, Yu H, Butterworth AS, Wang X, Mahajan A, Saleheen D, et al. Exome-wide association study of plasma lipids in >300,000 individuals. Nat Genet 2017;49:1758-1766.

16. Araki S, Okazaki M, Goto S. Impaired lipid metabolism in aged mice as revealed by fasting-induced expression of apolipoprotein mRNAs in the liver and changes in serum lipids. Gerontology 2004;50:206-215.
17. Wen Y, Liao G, Pritchard T, Zhao TT, Connelly JP, Pruett-Miller SM, Blanc V, et al. A Stable but Reversible Integrated Surrogate Reporter for Assaying CRISPR/Cas9-Stimulated Homology-directed Repair. J Biol Chem 2017.
18. Zhou J, Febbraio M, Wada T, Zhai Y, Kuruba R, He J, Lee JH, et al. Hepatic fatty acid transporter Cd36 is a common target of LXR, PXR, and PPARgamma in promoting steatosis. Gastroenterology 2008;134:556-567.
19. Zhou L, Xu L, Ye J, Li D, Wang W, Li X, Wu L, et al. Cidea promotes hepatic steatosis by sensing dietary fatty acids. Hepatology 2012;56:95-107.
20. Lee YJ, Ko EH, Kim JE, Kim E, Lee H, Choi H, Yu JH, et al. Nuclear receptor PPARgamma-regulated monoacylglycerol O-acyltransferase 1 (MGAT1) expression is responsible for the lipid accumulation in diet-induced hepatic steatosis. Proc Natl Acad Sci U S A 2012;109:13656-13661.
21. Yamanaka S, Balestra ME, Ferrell LD, Fan J, Arnold KS, Taylor S, Taylor JM, et al. Apolipoprotein B mRNA-editing protein induces hepatocellular carcinoma and dysplasia in transgenic animals. Proc Natl Acad Sci U S A 1995;92:8483-8487.
22. Yamanaka S, Poksay KS, Arnold KS, Innerarity TL. A novel translational repressor mRNA is edited extensively in livers containing tumors caused by the transgene expression of the apoB mRNA-editing enzyme. Genes Dev 1997;11:321-333.
23. Nikolaou KC, Vatandaslar H, Meyer C, Schmid MW, Tuschl T, Stoffel M. The RNA-Binding Protein A1CF Regulates Hepatic Fructose and Glycerol Metabolism via Alternative RNA Splicing. Cell Rep 2019;29:283-300 e288.
24. Li X, Qian X, Peng LX, Jiang Y, Hawke DH, Zheng Y, Xia Y, et al. A splicing switch from ketohexokinase-C to ketohexokinase-A drives hepatocellular carcinoma formation. Nat Cell Biol 2016;18:561-571.
25. Monga SP. beta-Catenin Signaling and Roles in Liver Homeostasis, Injury, and Tumorigenesis. Gastroenterology 2015;148:1294-1310.
26. Xu Q, Briggs J, Park S, Niu G, Kortylewski M, Zhang S, Gritsko T, et al. Targeting Stat3 blocks both HIF-1 and VEGF expression induced by multiple oncogenic growth signaling pathways. Oncogene 2005;24:5552-5560.
27. Szklarczyk D, Gable AL, Lyon D, Junge A, Wyder S, Huerta-Cepas J, Simonovic M, et al. STRING v11: protein-protein association networks with increased coverage, supporting functional discovery in genome-wide experimental datasets. Nucleic Acids Res 2019;47:D607-D613.
28. Madison BB, Liu Q, Zhong X, Hahn CM, Lin N, Emmett MJ, Stanger BZ, et al. LIN28B promotes growth and tumorigenesis of the intestinal epithelium via Let-7. Genes Dev 2013;27:2233-2245.
29. Lee AK, Ahn SG, Yoon JH, Kim SA. Sox4 stimulates ss-catenin activity through induction of CK2. Oncol Rep 2011;25:559-565.
30. Jiao Y, Zhao J, Zhang Z, Li M, Yu X, Yang Y, Liu J, et al. SRY-Box Containing Gene 4 Promotes Liver Steatosis by Upregulation of SREBP-1c. Diabetes 2018;67:2227-2238.
31. Vervoort SJ, van Boxtel R, Coffer PJ. The role of SRY-related HMG box transcription factor 4 (SOX4) in tumorigenesis and metastasis: friend or foe? Oncogene 2013;32:3397-3409.

32. Lourenco AR, Coffer PJ. SOX4: Joining the Master Regulators of Epithelial-to-Mesenchymal Transition? Trends Cancer 2017;3:571-582.
33. Li T, Liu X, Yang A, Fu W, Yin F, Zeng X. Associations of tumor suppressor SPARCL1 with cancer progression and prognosis. Oncol Lett 2017;14:2603-2610.
34. Tsukamoto S, Mizuta T, Fujimoto M, Ohte S, Osawa K, Miyamoto A, Yoneyama K, et al. Smad9 is a new type of transcriptional regulator in bone morphogenetic protein signaling. Sci Rep 2014;4:7596.
35. Pagadala M, Kasumov T, McCullough AJ, Zein NN, Kirwan JP. Role of ceramides in nonalcoholic fatty liver disease. Trends Endocrinol Metab 2012;23:365-371.
36. Esmaeili M MS, Tehrani G A. Evaluation of Additional Abcc12 Gene expression character in Breast cancer samples using Formal diagnostic profile. Gene Cell Tissue 2019.
37. Dominguez D, Freese P, Alexis MS, Su A, Hochman M, Palden T, Bazile C, et al. Sequence, Structure, and Context Preferences of Human RNA Binding Proteins. Mol Cell 2018;70:854-867 e859.
38. Sookoian S, Pirola CJ. Genetics of Nonalcoholic Fatty Liver Disease: From Pathogenesis to Therapeutics. Semin Liver Dis 2019;39:124-140.
39. de Vries PS, Brown MR, Bentley AR, Sung YJ, Winkler TW, Ntalla I, Schwander K, et al. Multiancestry Genome-Wide Association Study of Lipid Levels Incorporating Gene-Alcohol Interactions. Am J Epidemiol 2019;188:1033-1054.
40. Blanc V, Kennedy S, Davidson NO. A novel nuclear localization signal in the auxiliary domain of apobec-1 complementation factor regulates nucleocytoplasmic import and shuttling. J Biol Chem 2003;278:41198-41204.
41. Grohmann M, Wiede F, Dodd GT, Gurzov EN, Ooi GJ, Butt T, Rasmiena AA, et al. Obesity Drives STAT-1-Dependent NASH and STAT-3-Dependent HCC. Cell 2018;175:1289-1306 e1220.
42. Rodriguez FJ, Lewis-Tuffin LJ, Anastasiadis PZ. E-cadherin's dark side: possible role in tumor progression. Biochim Biophys Acta 2012;1826:23-31.
43. Matsumura T, Makino R, Mitamura K. Frequent down-regulation of E-cadherin by genetic and epigenetic changes in the malignant progression of hepatocellular carcinomas. Clin Cancer Res 2001;7:594-599.
44. Wei Y, Van Nhieu JT, Prigent S, Srivatanakul P, Tiollais P, Buendia MA. Altered expression of E-cadherin in hepatocellular carcinoma: correlations with genetic alterations, beta-catenin expression, and clinical features. Hepatology 2002;36:692-701.
45. Ghafoory S, Mehrabi A, Hafezi M, Cheng X, Breitkopf-Heinlein K, Hick M, Huichalaf M, et al. Nuclear accumulation of CDH1 mRNA in hepatocellular carcinoma cells. Oncogenesis 2015;4:e152.
46. Liu H, Hu J, Wei R, Zhou L, Pan H, Zhu H, Huang M, et al. SPAG5 promotes hepatocellular carcinoma progression by downregulating SCARA5 through modifying beta-catenin degradation. J Exp Clin Cancer Res 2018;37:229.
47. Sang X, Wu F, Wu D, Lin S, Li J, Zhao N, Chen X, et al. Human Hepatic Cancer Stem Cells (HCSCs) Markers Correlated With Immune Infiltrates Reveal Prognostic Significance of Hepatocellular Carcinoma. Front Genet 2020;11:112.
48. Blanc V, Henderson JO, Newberry EP, Kennedy S, Luo J, Davidson NO. Targeted deletion of the murine apobec-1 complementation factor (acf) gene results in embryonic lethality. Mol Cell Biol 2005;25:7260-7269.

49. Yang JD, Harmsen WS, Slettedahl SW, Chaiteerakij R, Enders FT, Therneau TM, Orsini L, et al. Factors that affect risk for hepatocellular carcinoma and effects of surveillance. Clin Gastroenterol Hepatol 2011;9:617-623 e611.
50. Vilar-Gomez E, Calzadilla-Bertot L, Wai-Sun Wong V, Castellanos M, Aller-de la Fuente R, Metwally M, Eslam M, et al. Fibrosis Severity as a Determinant of Cause-Specific Mortality in Patients With Advanced Nonalcoholic Fatty Liver Disease: A Multi-National Cohort Study. Gastroenterology 2018;155:443-457 e417.
51. Wobser H, Dorn C, Weiss TS, Amann T, Bollheimer C, Buttner R, Scholmerich J, et al. Lipid accumulation in hepatocytes induces fibrogenic activation of hepatic stellate cells. Cell Res 2009;19:996-1005.
52. Hirano K, Young SG, Farese RV, Jr., Ng J, Sande E, Warburton C, Powell-Braxton LM, et al. Targeted disruption of the mouse apobec-1 gene abolishes apolipoprotein B mRNA editing and eliminates apolipoprotein B48. J Biol Chem 1996;271:9887-9890.
53. Simonet WS, Bucay N, Lauer SJ, Taylor JM. A far-downstream hepatocyte-specific control region directs expression of the linked human apolipoprotein E and C-I genes in transgenic mice. J Biol Chem 1993;268:8221-8229.
54. Xie Y, Nassir F, Luo J, Buhman K, Davidson NO. Intestinal lipoprotein assembly in apobec-1-/- mice reveals subtle alterations in triglyceride secretion coupled with a shift to larger lipoproteins. Am J Physiol Gastrointest Liver Physiol 2003;285:G735-746.
55. Blanc V, Park E, Schaefer S, Miller M, Lin Y, Kennedy S, Billing AM, et al. Genome-wide identification and functional analysis of Apobec-1-mediated C-to-U RNA editing in mouse small intestine and liver. Genome Biol 2014;15:R79.
56. Ritchie ME, Silver J, Oshlack A, Holmes M, Diyagama D, Holloway A, Smyth GK. A comparison of background correction methods for two-colour microarrays. Bioinformatics 2007;23:2700-2707.
57. Smyth GK, Speed T. Normalization of cDNA microarray data. Methods 2003;31:265-273.
58. Dobin A, Davis CA, Schlesinger F, Drenkow J, Zaleski C, Jha S, Batut P, et al. STAR: ultrafast universal RNA-seq aligner. Bioinformatics 2013;29:15-21.
59. de Hoon MJ, Imoto S, Nolan J, Miyano S. Open source clustering software. Bioinformatics 2004;20:1453-1454.
60. Saldanha AJ. Java Treeview--extensible visualization of microarray data. Bioinformatics 2004;20:3246-3248.
61. Liao Y, Smyth GK, Shi W. featureCounts: an efficient general purpose program for assigning sequence reads to genomic features. Bioinformatics 2014;30:923-930.
62. Patro R, Duggal G, Love MI, Irizarry RA, Kingsford C. Salmon provides fast and bias-aware quantification of transcript expression. Nat Methods 2017;14:417-419.
63. Robinson MD, McCarthy DJ, Smyth GK. edgeR: a Bioconductor package for differential expression analysis of digital gene expression data. Bioinformatics 2010;26:139-140.
64. Ritchie ME, Phipson B, Wu D, Hu Y, Law CW, Shi W, Smyth GK. limma powers differential expression analyses for RNA-sequencing and microarray studies. Nucleic Acids Res 2015;43:e47.
65. Liu R, Holik AZ, Su S, Jansz N, Chen K, Leong HS, Blewitt ME, et al. Why weight? Modelling sample and observational level variability improves power in RNA-seq analyses. Nucleic Acids Res 2015;43:e97.

66. Huang da W, Sherman BT, Lempicki RA. Systematic and integrative analysis of large gene lists using DAVID bioinformatics resources. Nat Protoc 2009;4:44-57.
67. Huang da W, Sherman BT, Zheng X, Yang J, Imamichi T, Stephens R, Lempicki RA. Extracting biological meaning from large gene lists with DAVID. Curr Protoc Bioinformatics 2009;Chapter 13:Unit 13 11.

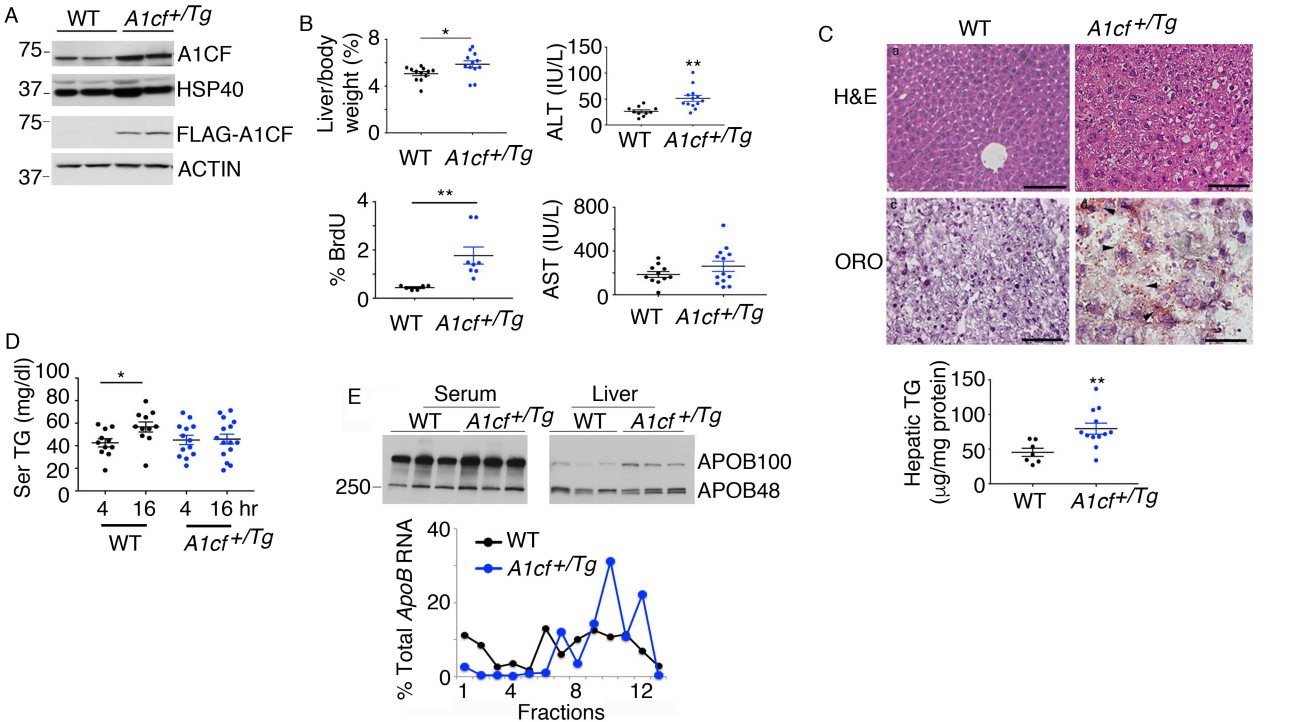
A
WT
A1cf+/Tg
75
A1CF
37
HSP40
75
FLAG-A1CF
37
ACTIN
B
Liver/body weight (%)
ALT (IU/L)
% BrdU
AST (IU/L)
WT
A1cf+/Tg
C
WT
A1cf+/Tg
H&E
ORO
Hepatic TG (μg/mg protein)
D
Ser TG (mg/dl)
4
16
4
16 hr
WT
A1cf+/Tg
E
Serum
Liver
APOB100
APOB48
250
% Total ApoB RNA
Fractions

Figure 1

Figure 1. Young (8-14 weeks) *A1cf* $^{+/Tg}$ mice on chow diet exhibit increased proliferation and hepatic steatosis. (**A**) Western blot of *A1cf* transgene expression in *A1cf* $^{+/Tg}$ liver using A1CF and FLAG antibodies. (**B**) Liver to whole body weight ratio of *A1cf* $^{+/Tg}$ mice, represented as mean ± SE, **P* < 0.05. Serum ALT and AST in *A1cf* $^{+/Tg}$ mice (11-13 per genotype). Data are shown as mean ± SE, ** *P* < 0.01. Proliferative index expressed as percent of BrdU-positive hepatocytes (mean ± SE, n=6-8) ** *P* < 0.01. (**C**) H&E and oil Red O-stained liver sections from *A1cf* $^{+/Tg}$ mice. Scale bars: 50 μm. Hepatic Triglyceride (TG) content (mean ± SE, 7-12 mice), ** *P* < 0.01. (**D**) Serum TG after 4 or 16 h fast (n=11-15 animals per group). Data are mean ± SE, * *P* < 0.05. (**E**) Western blot of serum and hepatic APOB. Lower panel, polysomal distribution of *ApoB* RNA upon fractionation of hepatic cytoplasmic extracts from *A1cf* $^{+/Tg}$ mice: monosome (fractions 1-6) and polysome (fractions 7-13). Data are representative of 4 separate isolations. Unpaired Student's t-test was used to determine significance between *A1cf* $^{+/Tg}$ and wild-type control groups for all experiments.

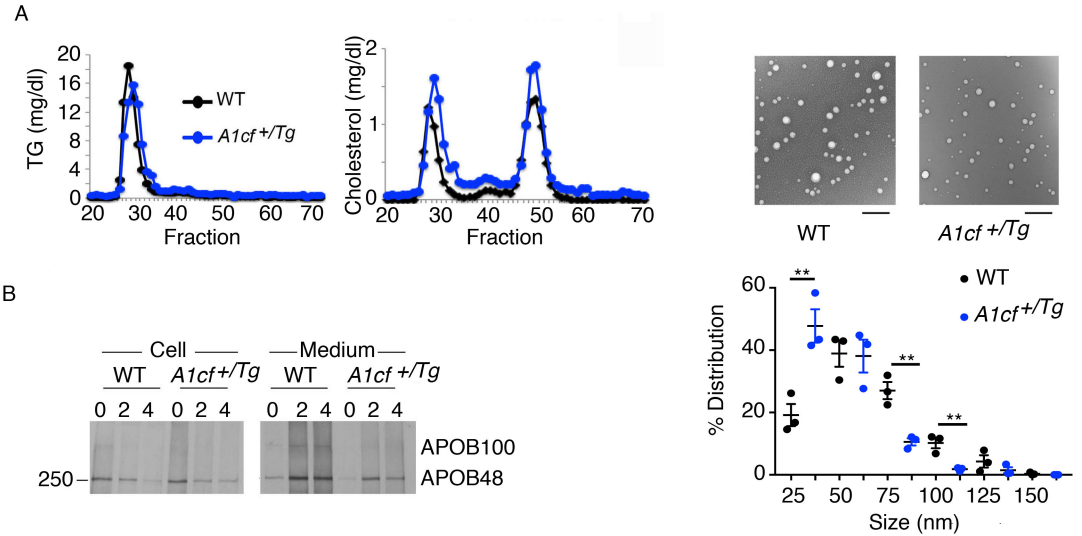
A
TG (mg/dl)
20
16
12
8
4
0
20 30 40 50 60 70
Fraction
WT
A1cf +/Tg
Cholesterol (mg/dl)
2
1
0
20 30 40 50 60 70
Fraction
WT
A1cf +/Tg
B
Cell
Medium
WT
A1cf +/Tg
WT
A1cf +/Tg
0 2 4 0 2 4 0 2 4 0 2 4
250
APOB100
APOB48
% Distribution
60
40
20
0
**
**
**
WT
A1cf +/Tg
25 50 75 100 125 150
Size (nm)

Figure 2

Figure 2. Young *A1cf* $^{+/Tg}$ mice show reduced APOB secretion and smaller VLDL particles. (**A**) Serum lipoprotein profile (n=4 per group) following a 4h fast and fractionation by fast protein liquid chromatography (FPLC). TG and cholesterol levels were biochemically determined. Right panel, Electron microscopy of serum VLDL particles isolated from pooled serum, 4 h after Pluronic F127 injection. Scale bars: 500 nm. Size distribution of VLDL particles is representative of 3 separate evaluations, ** $P <$ 0.01. (**B**) Pulse chase analysis of [^{35}S]-labeled APOB synthesis and secretion from primary hepatocytes isolated from *A1cf* $^{+/Tg}$ mice. Autoradiograph is a representative image of three independent experiments. Unpaired Student's t-test was used to determine significance between groups.

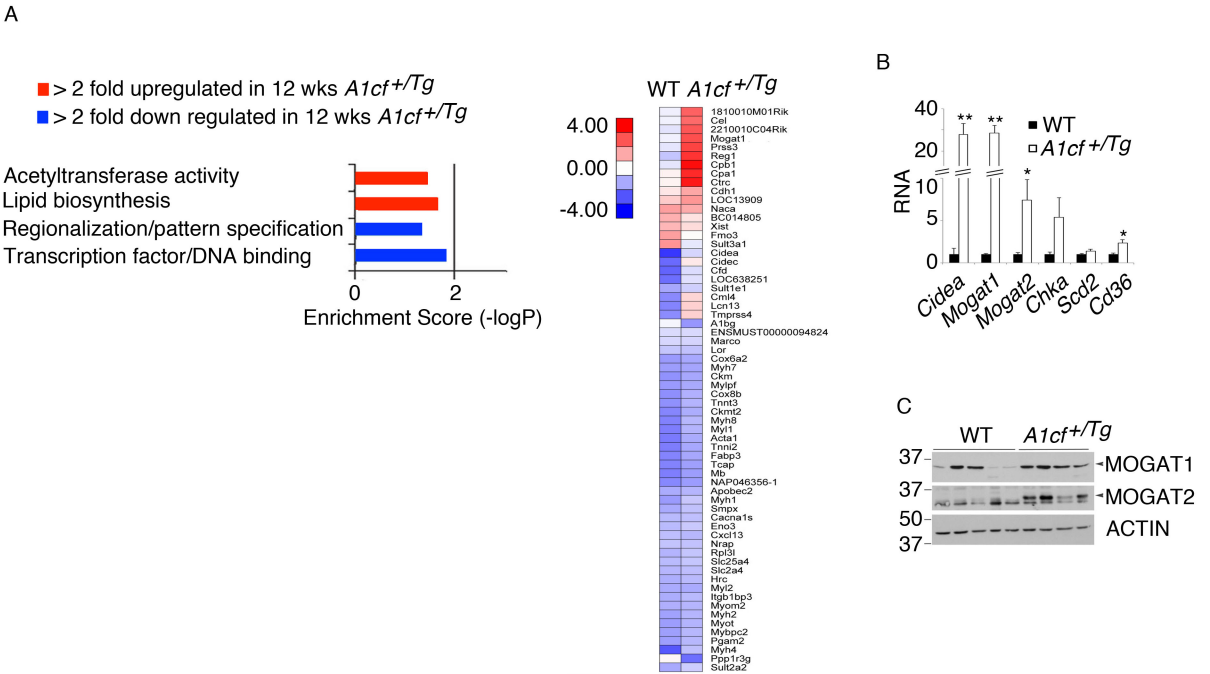
A
> 2 fold upregulated in 12 wks A1cf+/Tg
> 2 fold down regulated in 12 wks A1cf+/Tg
Acetyltransferase activity
Lipid biosynthesis
Regionalization/pattern specification
Transcription factor/DNA binding
0
2
Enrichment Score (-logP)
WT A1cf+/Tg
4.00
0.00
-4.00
1810010M01Rik
Cel
2210010C04Rik
Mogat1
Prss3
Reg1
Cpb1
Cpa1
Ctrc
Cdh1
LOC13909
Naca
BC014805
Xist
Fmo3
Sult3a1
Cidea
Cidec
Cfd
LOC638251
Sult1e1
Cml4
Lcn13
Tmprss4
A1bg
ENSMUST00000094824
Marco
Lor
Cox6a2
Myh7
Ckm
Mylpf
Cox8b
Tnnt3
Ckmt2
Myh8
Myl1
Acta1
Tnni2
Fabp3
Tcap
Mb
NAP046356-1
Apobec2
Myh1
Smpx
Cacna1s
Eno3
Cxcl13
Nrap
Rpl3l
Slc25a4
Slc2a4
Hrc
Myl2
Itgb1bp3
Myom2
Myh2
Myot
Mybpc2
Pgam2
Myh4
Ppp1r3g
Sult2a2
B
RNA
40
20
10
5
0
WT
A1cf+/Tg
Cidea
Mogat1
Mogat2
Chka
Scd2
Cd36
C
WT
A1cf+/Tg
37
37
50
37
MOGAT1
MOGAT2
ACTIN

Figure 3

Figure 3. Hepatic enrichment in genes involved in lipid biosynthesis in *A1cf* $^{+/Tg}$ mice. Expression profile of liver-enriched genes in 8-14 week chow-fed *A1cf* $^{+/Tg}$ mice**.** (**A**) Enriched KEGG pathways in differentially expressed genes from *A1cf* $^{+/Tg}$ livers. Heat-map diagram of the more than 2 fold differentially expressed genes in *A1cf* $^{+/Tg}$ mice. (**B**) QPCR validation of differentially up-regulated genes involved in lipid biosynthesis, n=6-7 mice per genotype; data are mean ± SE. Unpaired Student's t-test was used to determine significance between genotypes. ** $P < 0.01$, * $P < 0.05$. (**C**) Western blot analysis of MOGAT1 and MOGAT2 in livers from chow-fed *A1cf* $^{+/Tg}$ mice. ACTIN was used as loading control. (N=4-5 mice per genotype).

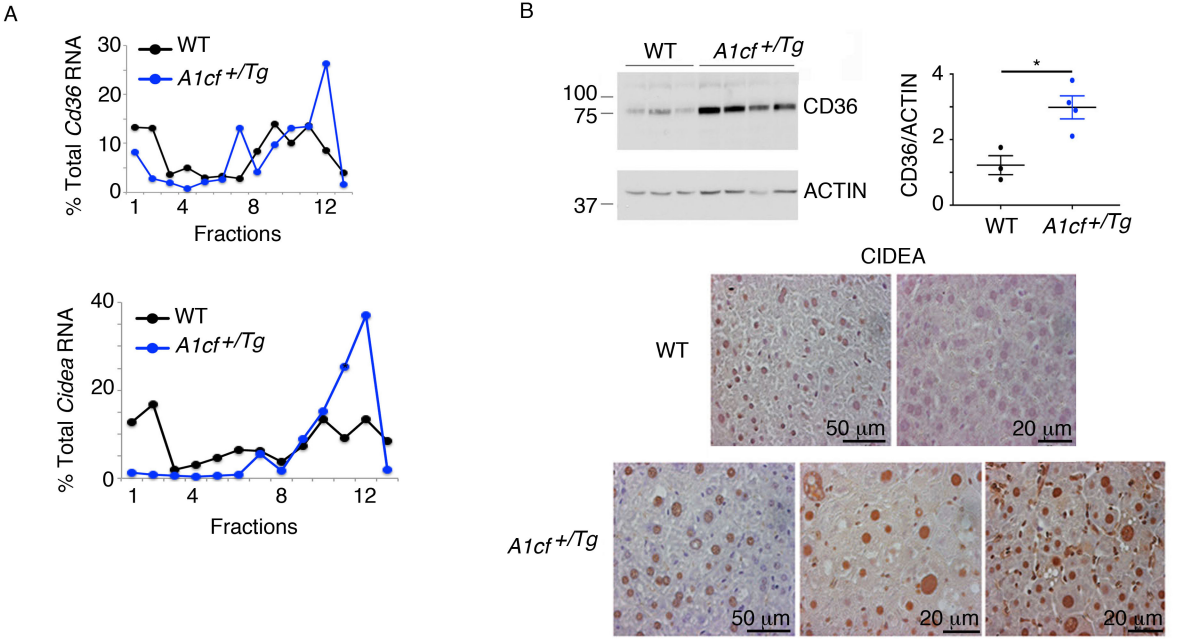
A
% Total Cd36 RNA
30
20
10
0
WT
A1cf+/Tg
1
4
8
12
Fractions
% Total Cidea RNA
40
20
0
WT
A1cf+/Tg
1
4
8
12
Fractions
B
WT
A1cf+/Tg
100
75
CD36
37
ACTIN
CD36/ACTIN
4
2
0
*
WT
A1cf+/Tg
CIDEA
WT
50 μm
20 μm
A1cf+/Tg
50 μm
20 μm
20 μm

Figure 4

Figure 4. Altered expression of genes promoting fatty acid uptake and lipogenesis in *A1cf* $^{+/Tg}$ mice. (**A**) Polysomal distribution of *Cd36* and *Cidea* RNAs from cytoplasmic extracts from *A1cf* $^{+/Tg}$ liver. RNA abundance was quantitated by QPCR across monosome (fractions 1-6) and polysome (fractions 7-13). Data are representative of 3 separate fractionations. (**B**) Western blot analysis of CD36 in liver of *A1cf* $^{+/Tg}$ mice using ACTIN as loading control. Data are mean ± SE. Significance was determined using unpaired Student's t-test, * $P < 0.05$. Immunohistochemical analysis of CIDEA in liver of *A1cf* $^{+/Tg}$ mice and littermate controls.

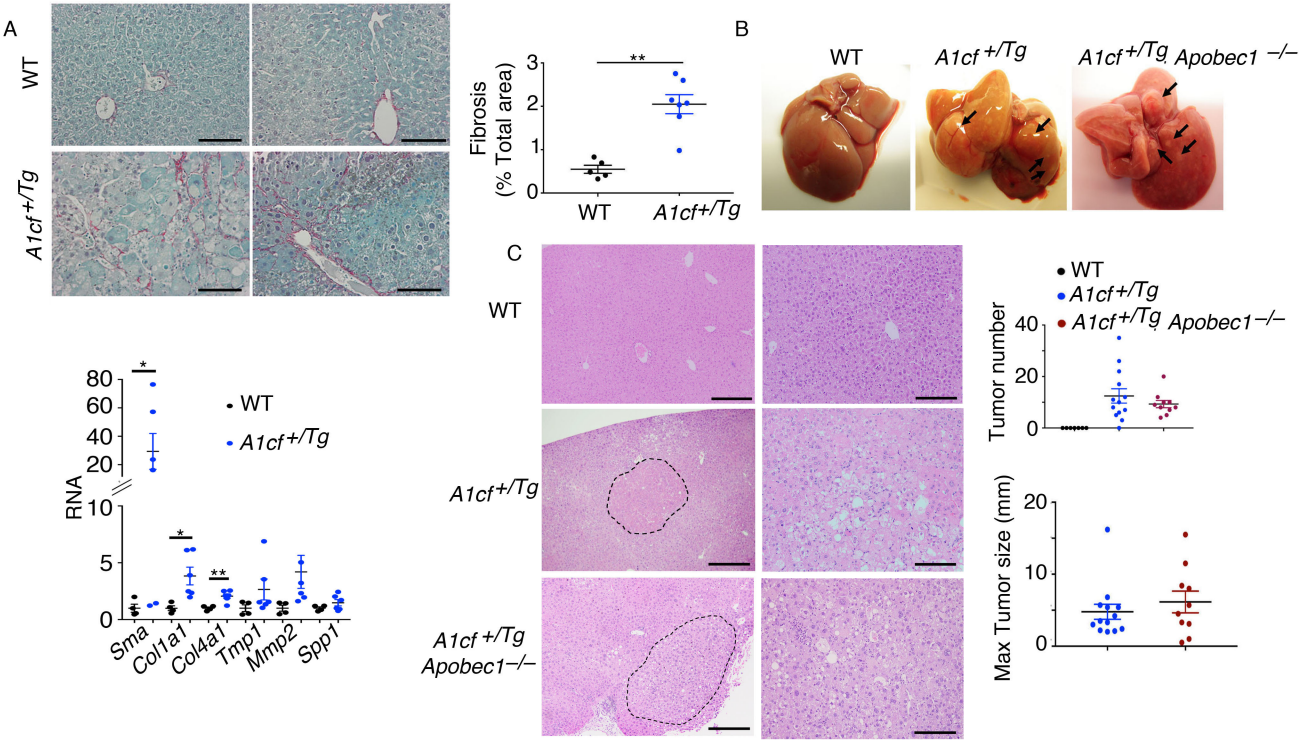
A
WT
A1cf+/Tg
Fibrosis (% Total area)
**
WT
A1cf+/Tg
B
WT
A1cf +/Tg
A1cf+/Tg Apobec1 −/−
C
WT
A1cf+/Tg
A1cf +/Tg Apobec1−/−
RNA
WT
A1cf+/Tg
Sma
Col1a1
Col4a1
Tmp1
Mmp2
Spp1
Tumor number
Max Tumor size (mm)

Figure 5

Figure 5. Hepatic overexpression of A1CF promotes fibrosis and spontaneous tumorigenesis. (**A**) Representative images of Sirius red-stained *A1cf* $^{+/Tg}$ and WT livers. Scale bars: 50 μm. Quantitation of Sirius red-stained area expressed as percent total area, (mean ± SE). Significance was determined using unpaired Student's t-test, ** $P <$ 0.01 (n=6). Lower panel, QPCR evaluation of fibrogenic genes in livers of chow-fed 12-month-old *A1cf* $^{+/Tg}$ mice; data are mean ± SE (n=6 per genotype). Unpaired t-test was used to determine significance between 12-month-old groups. * $P < 0.05$. (**B**) Gross images of liver from *A1cf* $^{+/Tg}$ and *A1cf* $^{+/Tg}$ *Apobec1* $^{-/-}$ mice at 12 months of age fed a low fat chow diet. (**C**) Representative images of H&E- stained liver sections from *A1cf* $^{+/Tg}$ and *A1cf* $^{+/Tg}$ *Apobec1*$^{-/-}$ mice. The dashed curved lines delineate tumor margin. Scale bars: 100 μm (left) and 50 μm (right). Macroscopic quantitation and size of nodules showing total number (top panel) and maximum size (mm) of tumors (lower panel).

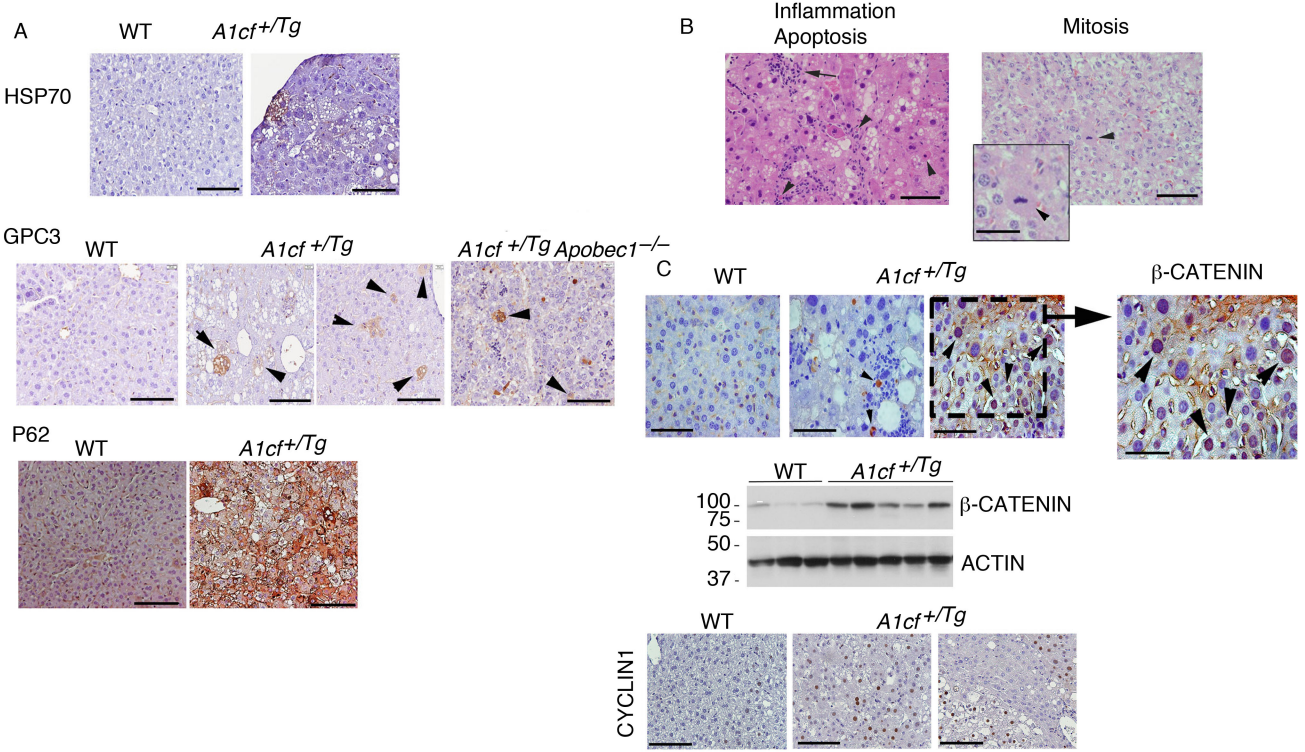
A
WT
A1cf+/Tg
HSP70
GPC3
WT
A1cf +/Tg
A1cf +/Tg Apobec1−/−
P62
WT
A1cf+/Tg
B
Inflammation
Apoptosis
Mitosis
C
WT
A1cf+/Tg
β-CATENIN
WT
A1cf+/Tg
100
75
50
37
β-CATENIN
ACTIN
WT
A1cf+/Tg
CYCLIN1

Figure 6

Figure 6. Increased expression of HCC markers in 12-month-old *A1cf* $^{+/Tg}$ mice.
(**A**) Representative images of HSP70 and p62 expression in HCC from 12 month-old *A1cf* $^{+/Tg}$ mice. Representative images of hepatic GPC3 in 12-month-old *A1cf* $^{+/Tg}$ and *A1cf* $^{+/Tg}$ *Apobec1* $^{-/-}$ mice. Arrows indicate clusters of GPC3-positive cells. (**B**) Representative H&E images of pathological features identified in 12-month-old *A1cf* $^{+/Tg}$ liver. Left panel, arrow indicates focal inflammation. Arrowheads indicate apoptotic cells. Right panel, arrowhead indicates mitotic body. (**C**)**.** Immunohistochemical staining of 12 month-old *A1cf* $^{+/Tg}$ livers with β-CATENIN antibody. Expression of β-CATENIN in liver tissue from *A1cf* $^{+/Tg}$ and littermate controls evaluated by western blot and compared to ACTIN. Representative images of CYCLIN D1 in liver from 12 month-old *A1cf* $^{+/Tg}$ mice. All panels, scale bars: 50 μm.

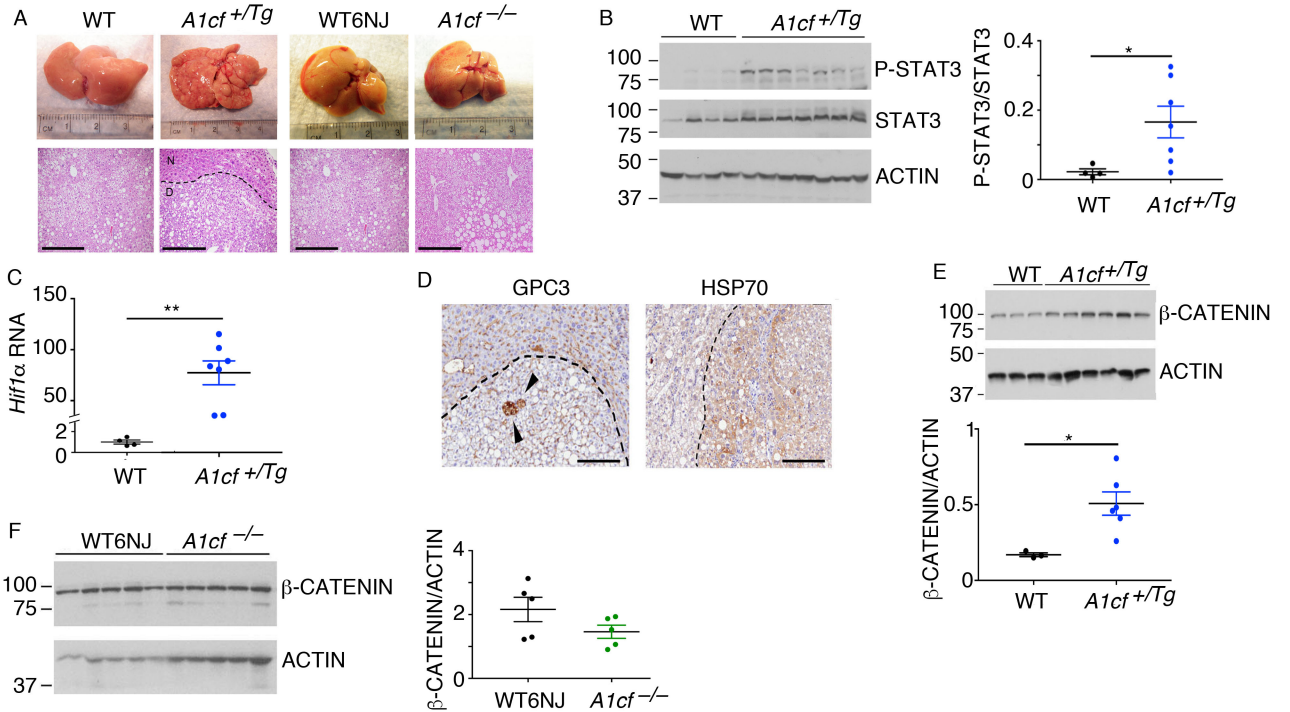
A
WT
A1cf +/Tg
WT6NJ
A1cf −/−
N
D
B
WT
A1cf +/Tg
100
75
P-STAT3
100
75
STAT3
50
37
ACTIN
P-STAT3/STAT3
0.4
0.2
0
*
WT
A1cf +/Tg
C
Hif1α RNA
150
100
50
2
0
**
WT
A1cf +/Tg
D
GPC3
HSP70
E
WT
A1cf+/Tg
100
75
β-CATENIN
50
37
ACTIN
β-CATENIN/ACTIN
1
0.5
0
*
WT
A1cf +/Tg
F
WT6NJ
A1cf −/−
100
75
β-CATENIN
37
ACTIN
β-CATENIN/ACTIN
4
2
0
WT6NJ
A1cf −/−

Figure 7

Figure 7. Accelerated hepatic tumorigenesis in *A1cf* $^{+/Tg}$ mice fed a transfat/fructose diet (TFF). (**A**) Upper panel, gross images of liver from *A1cf* $^{+/Tg}$ and *A1cf* $^{-/-}$ mice fed TFF diet for 6 months. Lower panel show H&E staining revealing fat accumulation in all genotypes but dysplastic nodules (dashed area) only in *A1cf* $^{+/Tg}$ liver. Scale bars: 100 μm. (**B**) Western blot analysis of STAT3 activation/phosphorylation at Tyr 705. P-STAT3 was normalized to total STAT3 (n=7 *A1cf* $^{+/Tg}$ and 4 WT). Unpaired Student's t-test was used to determine significance between groups, * $P < 0.05$. (**C**)**.** Expression of STAT3 downstream target, *Hif1α* RNA by QPCR. Data are mean ± SE (n=7 *A1cf* $^{+/Tg}$ and 4 WT). ** $P < 0.01$ determined by unpaired Student's t-test. (**D**) Representative images of GPC3 and HSP70-stained sections from *A1cf* $^{+/Tg}$ mice. Distinct nodules are delineated by dashed curved lines. GPC3 staining shows rare cells staining with cytoplasmic positivity within the nodule (arrowheads). Positive HSP70 staining in liver nodule, supporting neoplastic progression. Scale bars: 50 μm. (**E-F**) Expression of β-CATENIN in liver from 7 *A1cf* $^{+/Tg}$ and 4 WT mice (E) and 5 *A1cf* $^{-/-}$ mice and 5 aged-matched WT6NJ mice (F). Expression of β-CATENIN normalized to ACTIN is shown as β-CATENIN/ACTIN ratio. Significance was determined using unpaired Student's t-test * $P < 0.05$.

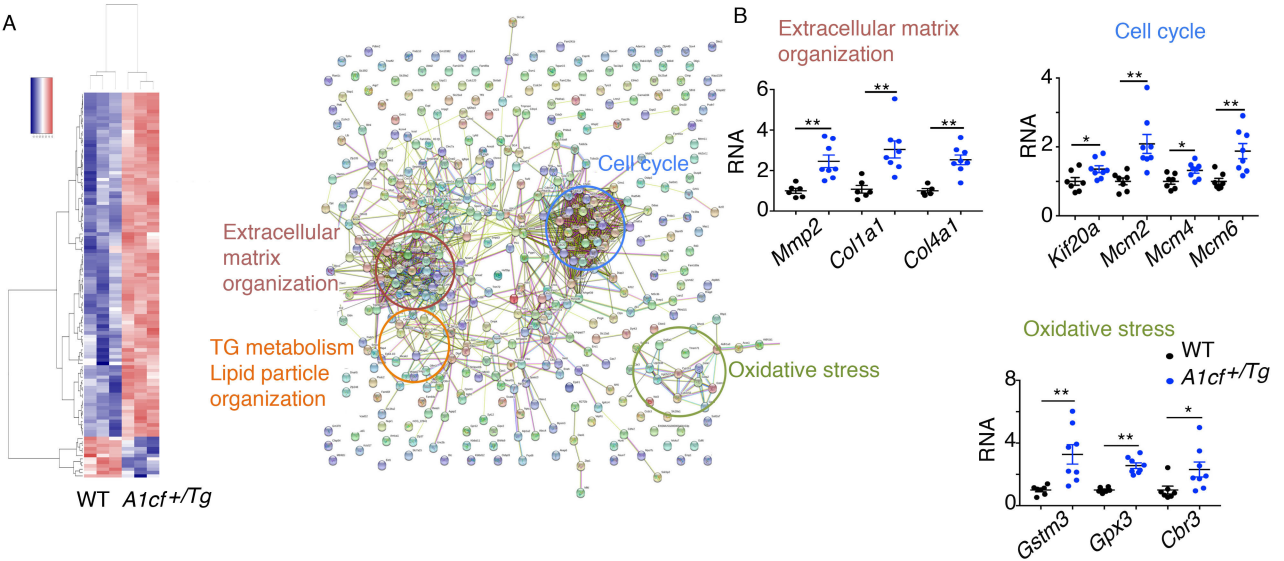
A
WT
A1cf+/Tg
Cell cycle
Extracellular matrix organization
TG metabolism Lipid particle organization
Oxidative stress
B
Extracellular matrix organization
RNA
Mmp2
Col1a1
Col4a1
Cell cycle
Kif20a
Mcm2
Mcm4
Mcm6
Oxidative stress
WT
A1cf+/Tg
Gstm3
Gpx3
Cbr3

Figure 8

Figure 8. Differentially expressed genes in livers from young *A1cf* $^{+/Tg}$ mice**.** (**A**) Heatmap of the 556 differentially expressed genes. STRING analysis of the differentially expressed genes showing enriched pathways. (**B**) QPCR validation of gene clusters involved in extracellular matrix organization (red), cell cycle (blue) and oxidative stress (green); Data are mean ± SE n=6-8, * $P< 0.05$; ** $P< 0.01$ (unpaired t-test).

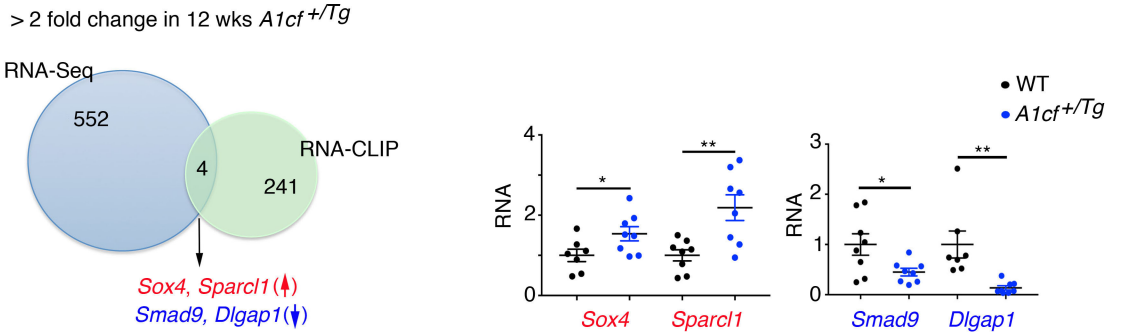
> 2 fold change in 12 wks A1cf +/Tg
RNA-Seq
552
4
RNA-CLIP
241
Sox4, Sparcl1 (↑)
Smad9, Dlgap1 (↓)
WT
A1cf +/Tg
RNA
4
2
0
*
**
Sox4
Sparcl1
RNA
3
2
1
0
*
**
Smad9
Dlgap1

Figure 9

Figure 9. Schematic representation of differentially expressed genes in young *A1cf* $^{+/Tg}$ mice in relation to A1CF RNA-CLIP targets. Two A1CF RNA targets (*Sox4*, *Sparcl1*) are up-regulated (red), two (*Smad9*, *Dlgap1*) are down-regulated (blue) in *A1cf* $^{+/Tg}$ liver. Expression of those 4 targets was validated by QPCR (n=7-8) and shown as mean ± SE, * $P< 0.05$; ** $P< 0.01$ (unpaired t-test).

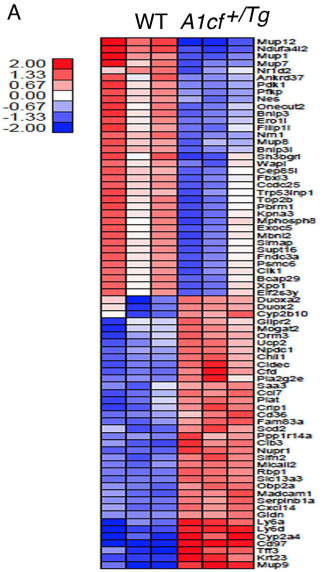
A
WT
A1cf+/Tg
2.00
1.33
0.67
0.00
-0.67
-1.33
-2.00
Mup12
Ndufa4l2
Mup1
Mup7
Nr1d2
Ankrd37
Pdk1
Pfkp
Nes
Oneout2
Bnip3
Ero1l
Fitp1l
Nrn1
Mup8
Bnip3l
Sh3bgrl
Wap
Cep65l
Fbxl3
Ccdc25
Trps3inp1
Top2b
Pprm1
Kpna3
Mphosph8
Exoc5
Mbnl2
Slmap
Supt16
Fndc3a
Psmc6
Clk1
Bcap29
Xpo1
Ehf2e3y
Duox2
Duoxa2
Cyp2b10
Gfpt2
Mcpt2
Orm3
Ucn2
Ndrg1
Chit1
Cidec
Cfd
Pla2g2e
Saa3
Ccl7
Plat
Cdp1
Cd36
Fam63a
Sod2
Ppp1r14a
Clb3
Nupr1
Slfn2
Micall2
Rbp1
Slc13a3
Obp2a
Madcam1
Serpinb1a
Cxcl14
Gldn
Ly6a
Ly6d
Gyp2a4
Cd97
Tff3
Krt23
Mup9

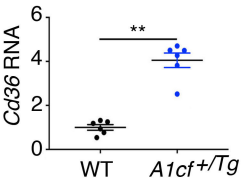
Cd36 RNA
6
4
2
0
**
WT
A1cf+/Tg

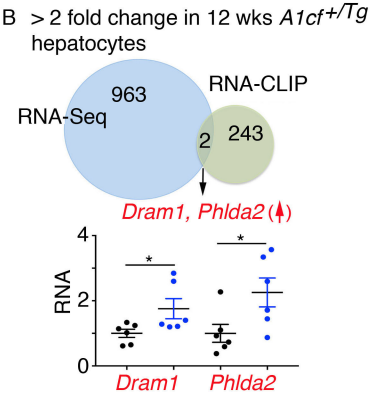
B > 2 fold change in 12 wks A1cf+/Tg hepatocytes
963
RNA-Seq
RNA-CLIP
2
243
Dram1, Phlda2 (▲)
RNA
4
2
0
*
*
Dram1
Phlda2

Figure 10

Figure 10. Differentially expressed genes in primary hepatocytes from young *A1cf* $^{+/Tg}$ mice in relation to A1CF RNA-CLIP targets. (**A**) Heatmap of 966 differentially altered genes in primary hepatocytes from *A1cf* $^{+/Tg}$ mice. Up-regulation of *Cd36* RNA in *A1cf* $^{+/Tg}$ hepatocytes represented as mean ± SE, (n=6) ** $P< 0.01$ (unpaired t-test). (**B**) Venn diagram showing two A1CF RNA-CLIP targets (*Dram1*, *Phlda2*), up-regulated in *A1cf* $^{+/Tg}$ hepatocytes with mRNA expression, validated by QPCR, shown as mean ± SE (n=6), * $P< 0.05$ (unpaired t-test).

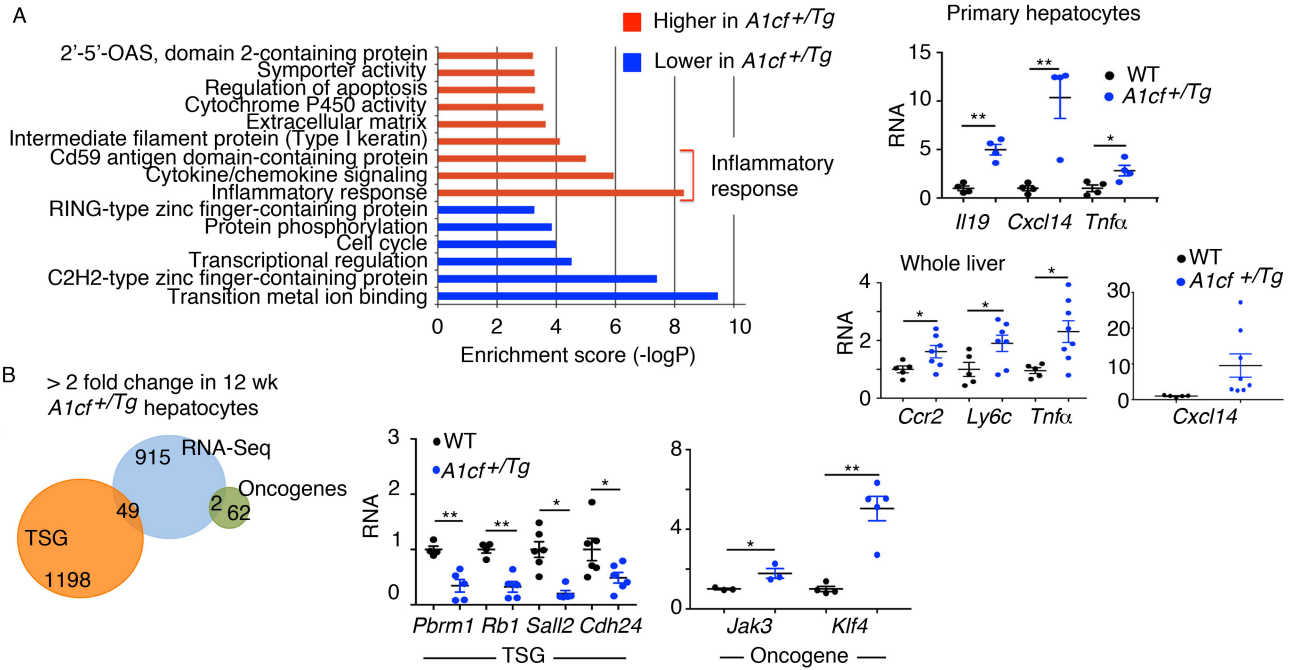
A
Higher in A1cf+/Tg
Lower in A1cf+/Tg
2'-5'-OAS, domain 2-containing protein
Symporter activity
Regulation of apoptosis
Cytochrome P450 activity
Extracellular matrix
Intermediate filament protein (Type I keratin)
Cd59 antigen domain-containing protein
Cytokine/chemokine signaling
Inflammatory response
RING-type zinc finger-containing protein
Protein phosphorylation
Cell cycle
Transcriptional regulation
C2H2-type zinc finger-containing protein
Transition metal ion binding
Inflammatory response
0 2 4 6 8 10
Enrichment score (-logP)
Primary hepatocytes
RNA
WT
A1cf+/Tg
Il19 Cxcl14 Tnfα
Whole liver
Ccr2 Ly6c Tnfα
Cxcl14
B
> 2 fold change in 12 wk
A1cf+/Tg hepatocytes
915 RNA-Seq
Oncogenes
49
2
62
TSG
1198
Pbrm1 Rb1 Sall2 Cdh24
TSG
Jak3 Klf4
Oncogene

Figure 11

Figure 11. *A1cf* $^{+/Tg}$ primary hepatocytes show enrichment in inflammatory response pathways. (**A**) Gene ontology analysis showing functional pathways over-represented (red) and under-represented (blue) in *A1cf* $^{+/Tg}$ hepatocytes. Relative expression of genes involved in inflammatory response examined by QPCR, both in isolated hepatocytes and whole liver (5-8 per genotype). Data are mean ± SE, * $P < 0.05$; ** $P < 0.01$ (unpaired t-test). (**B**) Venn diagram representing comparative analysis between genes with differentially altered expression in *A1cf* $^{+/Tg}$ hepatocytes and Tumor Suppressor Gene (TSG) and Oncogene databases. QPCR validation of a subset of TSG and oncogene RNAs from 4 to 5 independent hepatocyte isolations per genotype. Data are mean ± SE, * $P < 0.05$; ** $P < 0.01$ (unpaired t-test).

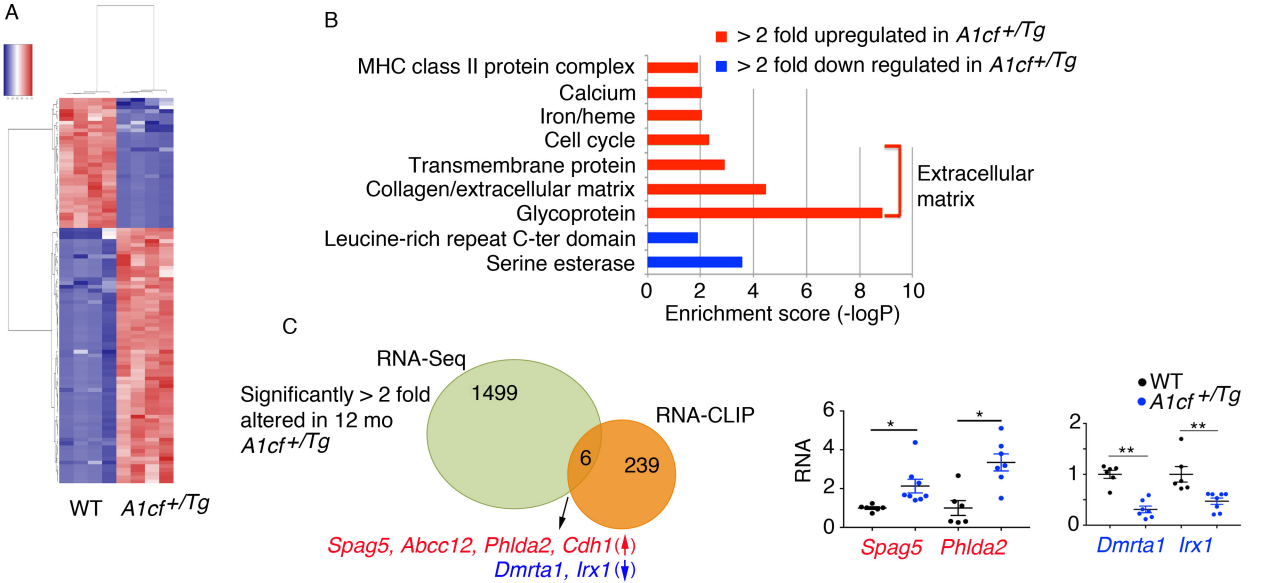
A
WT
A1cf+/Tg
B
> 2 fold upregulated in A1cf+/Tg
> 2 fold down regulated in A1cf+/Tg
MHC class II protein complex
Calcium
Iron/heme
Cell cycle
Transmembrane protein
Collagen/extracellular matrix
Glycoprotein
Leucine-rich repeat C-ter domain
Serine esterase
Extracellular matrix
0
2
4
6
8
10
Enrichment score (-logP)
C
RNA-Seq
Significantly > 2 fold altered in 12 mo A1cf+/Tg
1499
6
239
RNA-CLIP
Spag5, Abcc12, Phlda2, Cdh1
Dmrta1, Irx1
RNA
Spag5
Phlda2
WT
A1cf+/Tg
Dmrta1
Irx1

Figure 12

Figure 12. Summary of differentially expressed genes in liver of 12-month-old chow-fed *A1cf* $^{+/Tg}$ mice. (**A**) Heatmap showing expression of 1505 differentially expressed genes in *A1cf* $^{+/Tg}$ liver. (**B**) Gene Ontology analysis depicting functional categories over-represented (red bars) and under-represented (blue bars) in *A1cf* $^{+/Tg}$ livers. (**C**)**.** Venn diagram summarizing comparative analysis between 1505 differentially altered genes in *A1cf* $^{+/Tg}$ liver and A1CF RNA targets identified by RNA-CLIP. Six A1CF RNA targets showed altered expression, with four (*Spag5*, *Abcc12*, *Phlda2*, *Cdh1*) up-regulated (indicated in red) and two (*Dmrta1*, *Irx1*) down-regulated (indicated in blue). Expression was confirmed by QPCR (6-8 animals per genotype). Data indicate mean ± SE, * P <0.01; ** $P < 0.05$ (unpaired t-test).

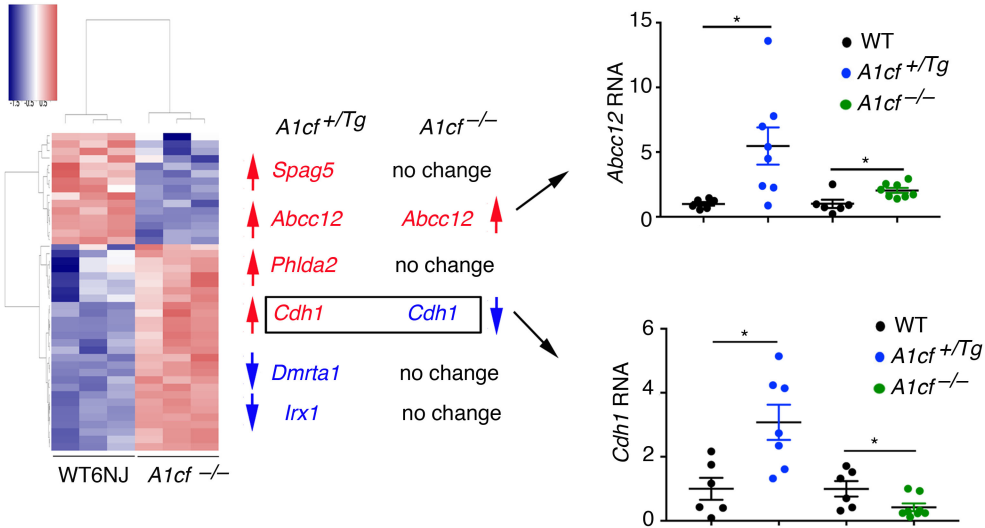
A1cf +/Tg
A1cf −/−
Spag5
no change
Abcc12
Abcc12
Phlda2
no change
Cdh1
Cdh1
Dmrta1
no change
Irx1
no change
WT6NJ
A1cf −/−
Abcc12 RNA
15
10
5
0
WT
A1cf +/Tg
A1cf −/−
Cdh1 RNA
6
4
2
0

Figure 13

Figure 13. Expression profile of differentially expressed A1CF RNA-CLIP targets in 12-month-old *A1cf* $^{-/-}$ mice**.** Heatmap representation of 298 genes with altered expression in liver of 12-month-old chow fed *A1cf* $^{-/-}$ mice. Expression of A1CF RNA targets, differentially expressed in 12-month-old *A1cf* $^{+/Tg}$, in liver of 12-month-old *A1cf* $^{-/-}$ mice. Genes up-regulated in aged *A1cf* $^{+/Tg}$ mice are indicated in red; genes down-regulated are indicated in blue. RNA-Seq analysis showed that of the six genes identified from RNA-Seq and RNA-CLIP in *A1cf* $^{+/Tg}$ mice, only *Cdh1* was ***both*** up-regulated in *A1cf* $^{+/Tg}$ mice **and** down-regulated in *A1cf* $^{-/-}$ mice. *Cdh1* RNA expression in *A1cf* $^{+/Tg}$ and *A1cf* $^{-/-}$ liver was confirmed by QPCR (N=6-7 per genotype). Data represent mean ± SE, * $P < 0.05$ (unpaired t-test).

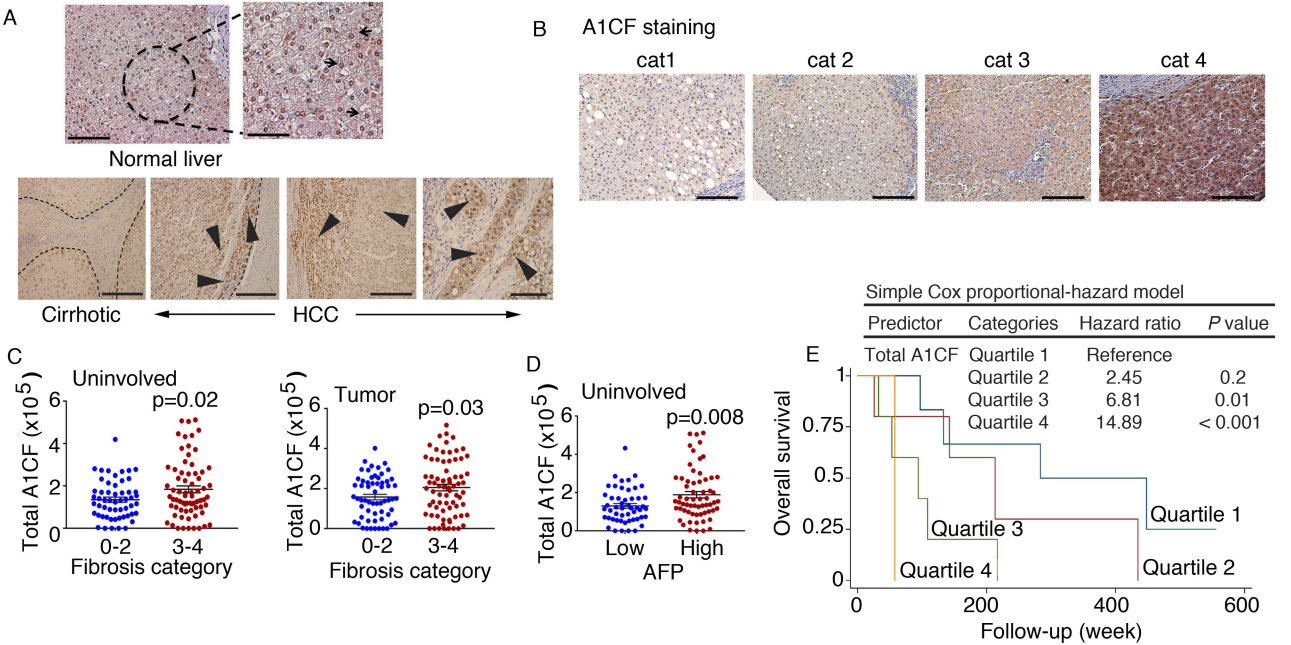
A
Normal liver
Cirrhotic
HCC
B
A1CF staining
cat1
cat 2
cat 3
cat 4
C
Uninvolved
p=0.02
Total A1CF (x10^5)
0-2
3-4
Fibrosis category
Tumor
p=0.03
Total A1CF (x10^5)
0-2
3-4
Fibrosis category
D
Uninvolved
p=0.008
Total A1CF (x10^5)
Low
High
AFP
E
Simple Cox proportional-hazard model
Predictor Categories Hazard ratio P value
Total A1CF Quartile 1 Reference
Quartile 2 2.45 0.2
Quartile 3 6.81 0.01
Quartile 4 14.89 < 0.001
Overall survival
Follow-up (week)
Quartile 1
Quartile 2
Quartile 3
Quartile 4

Figure 14

Figure 14. A1CF expression inferred from immunohistochemical staining in human HCC tissue microarray. (**A**) Top panel, A1CF staining of normal human liver showing homogenous strong nuclear expression. Scale bars: 50 μm. Lower panel, A1CF in cirrhotic and HCC tissue. Staining shows a gradient of expression with strong nuclear A1CF staining at the edge of cirrhotic nodules and tumor (arrowheads). Scale bars: first 3 panels 50 μm, last panel 20 μm. (**B**) A1CF expression in 137 human samples from a tissue microarray. Samples were categorized according to A1CF staining evaluated by quantitating pixels (see Methods). A representative image of each category is shown. Scale bars: 50 μm. (**C**) A1CF expression and comparison among fibrosis categories in uninvolved and tumor tissues from all patients. Data represent mean ± SE (unpaired t-test). (**D**) A1CF expression in uninvolved tissue and comparison among patients with low and high levels of AFP, represented as mean ± SE (unpaired t-test). (**E**)**.** Kaplan-Meier plots of the overall survival rates in HCC subjects with underlying NAFLD, stratified by A1CF staining intensity. Patients were divided into four quartiles based on A1CF total expression in uninvolved tissue. Patients with highest A1CF staining (quartile 4) show significantly reduced survival compared to patients with lower A1CF staining intensity (quartiles 1-3). Inset shows Cox proportional hazard values.

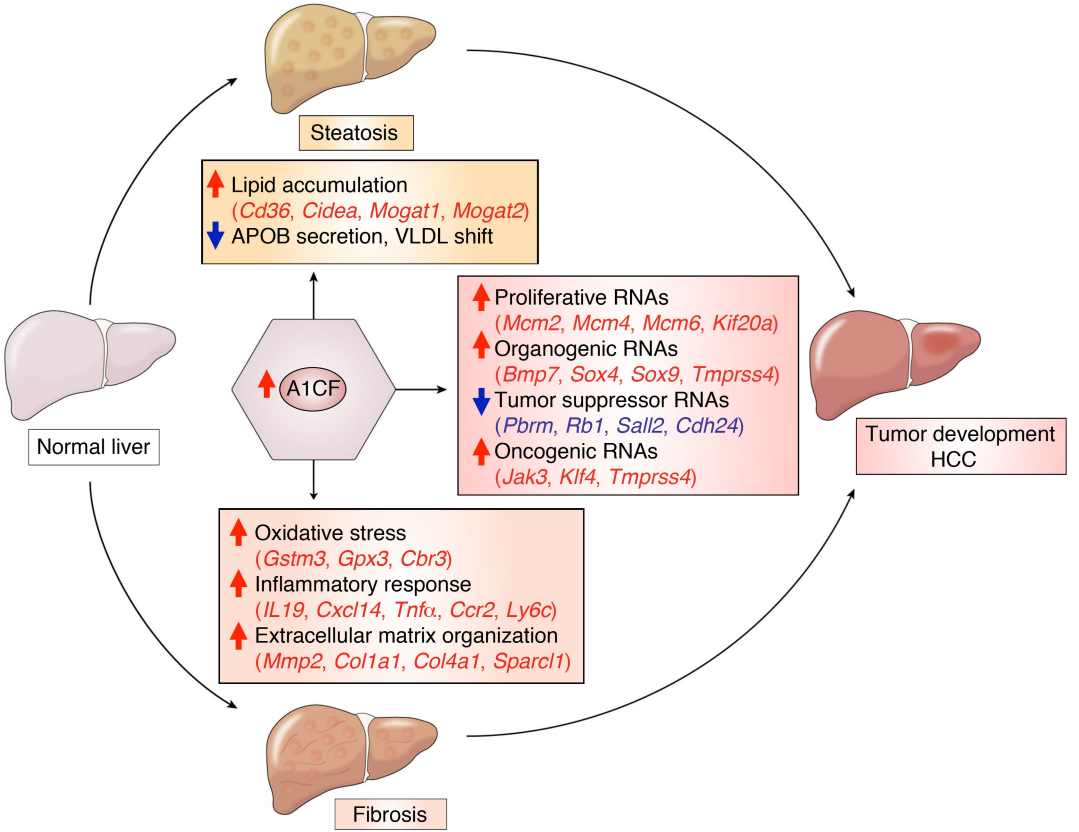
Steatosis
Lipid accumulation
(Cd36, Cidea, Mogat1, Mogat2)
APOB secretion, VLDL shift
Normal liver
A1CF
Proliferative RNAs
(Mcm2, Mcm4, Mcm6, Kif20a)
Organogenic RNAs
(Bmp7, Sox4, Sox9, Tmprss4)
Tumor suppressor RNAs
(Pbrm, Rb1, Sall2, Cdh24)
Oncogenic RNAs
(Jak3, Klf4, Tmprss4)
Tumor development
HCC
Oxidative stress
(Gstm3, Gpx3, Cbr3)
Inflammatory response
(IL19, Cxcl14, Tnfα, Ccr2, Ly6c)
Extracellular matrix organization
(Mmp2, Col1a1, Col4a1, Sparcl1)
Fibrosis

Figure 15

Figure 15. Schematic summary of findings with an integrated mechanism for A1CF-induced hepatic carcinogenesis. Hepatic overexpression of A1CF induces steatosis via pathways including increased expression of lipogenic genes, increased fatty acid/lipid uptake (*Cidea*, *Mogat1*, *Mogat2*, *Cd36*) and reduced VLDL APOB secretion. Increased A1CF expression is also associated with increased oxidative stress (*Gstm3*, *Gpx3*, *Cbr3*) an augmented inflammatory response (*Il19*, *Cxcl14*, *Tnfα*, *Ccr2*, *Ly6c*) and exaggerated extracellular matrix organization (*Mmp2*, *Col1a1*, *Col4a1*, *Sparcl1*), which together promote accumulation of collagen and fibrosis. In parallel, hepatic overexpression of A1CF increases expression of proliferative genes (*Mcm2*, *Mcm4*, *Mcm6*, *Kif20a*), organogenic genes (*Bmp7*, *Sox4*, *Sox9*, *Tmprss4*), oncogenic genes (*Jak3*, *Klf4*, *Tmprss4*) and decreases expression of tumor suppressor genes (*Pbrm1*, *Rb1*, *Sall2*, *Cdh24*). These adaptive responses, including steatosis, fibrosis and augmented proliferation combine to promote spontaneous hepatic carcinogenesis in *A1cf* $^{+/Tg}$ mice.

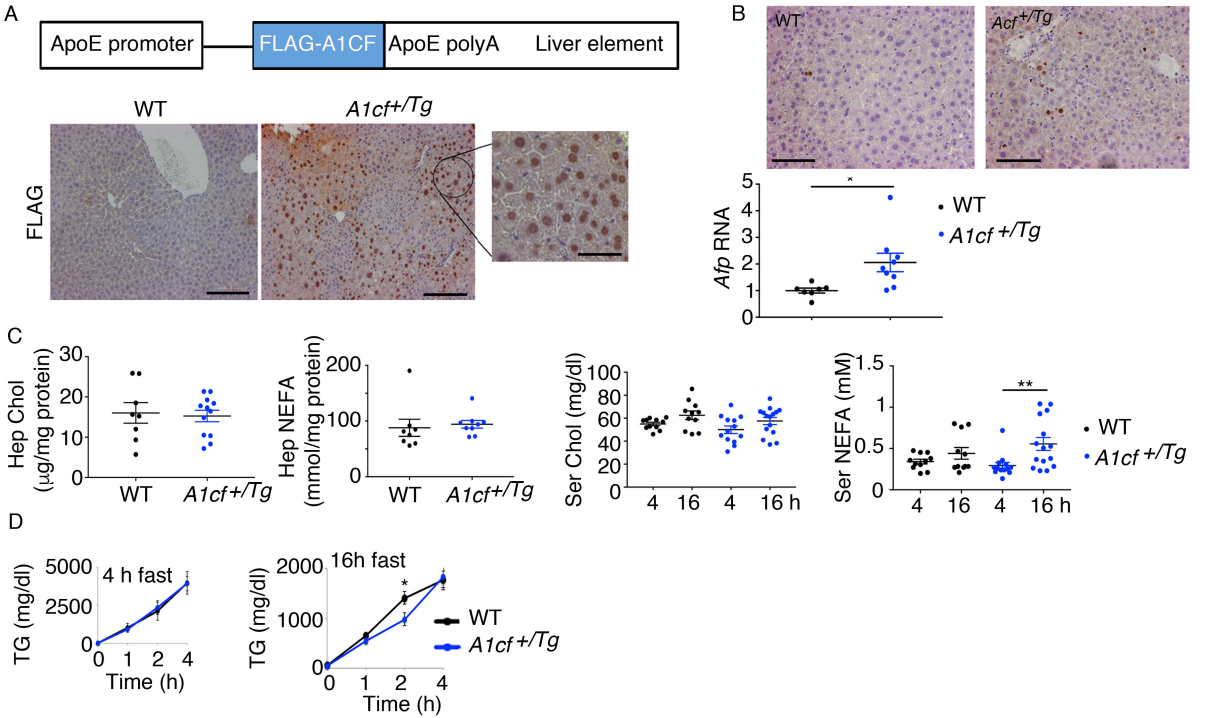

Supplemental Figure 1

Supplemental Figure 1. Baseline characterization of 12-week-old chow fed *A1cf* $^{+/Tg}$ mice. (**A**) Diagram of the ApoE-A1cf transgenic construct. *A1cf* transgene is expressed as a N-terminal FLAG-tagged protein. A1CF transgene is detectable by immunohistochemistry using anti-FLAG antibody and appears highly expressed in nuclear compartment of hepatocytes. Scale bars: main panel: 100 μm; inset: 50 μm. (**B**) Representative images of proliferative hepatocytes labeled with BrdU in *A1cf* $^{+/Tg}$ mice (related to Figure 1B) Scale bars: 50 μm. Hepatic *Afp* RNA expression in *A1cf* $^{+/Tg}$ mice evaluated by QPCR (n=7-9 animals per genotype). Data are mean ± SE. * $P < 0.05$ (unpaired t-test). (**C**) Hepatic cholesterol and NEFA content were determined biochemically and normalized to hepatic protein. Values are means ± SE from 8-12 mice per genotype. Biochemical determination of serum cholesterol and NEFA in chow-fed *A1cf* $^{+/Tg}$ mice after a 4 or 16 h fast; n=11-15 animals per genotype and fasting condition. Data are means ± SE, ** $P < 0.01$ (unpaired t-test). (**D**) Plasma VLDL-TG secretion rate in *A1cf* $^{+/Tg}$ mice fasted for 4 or 16 h and injected with Pluronic F-127. Each point represents mean ± SE (n=2-6 mice per genotype) * $P < 0.05$ (unpaired t-test).

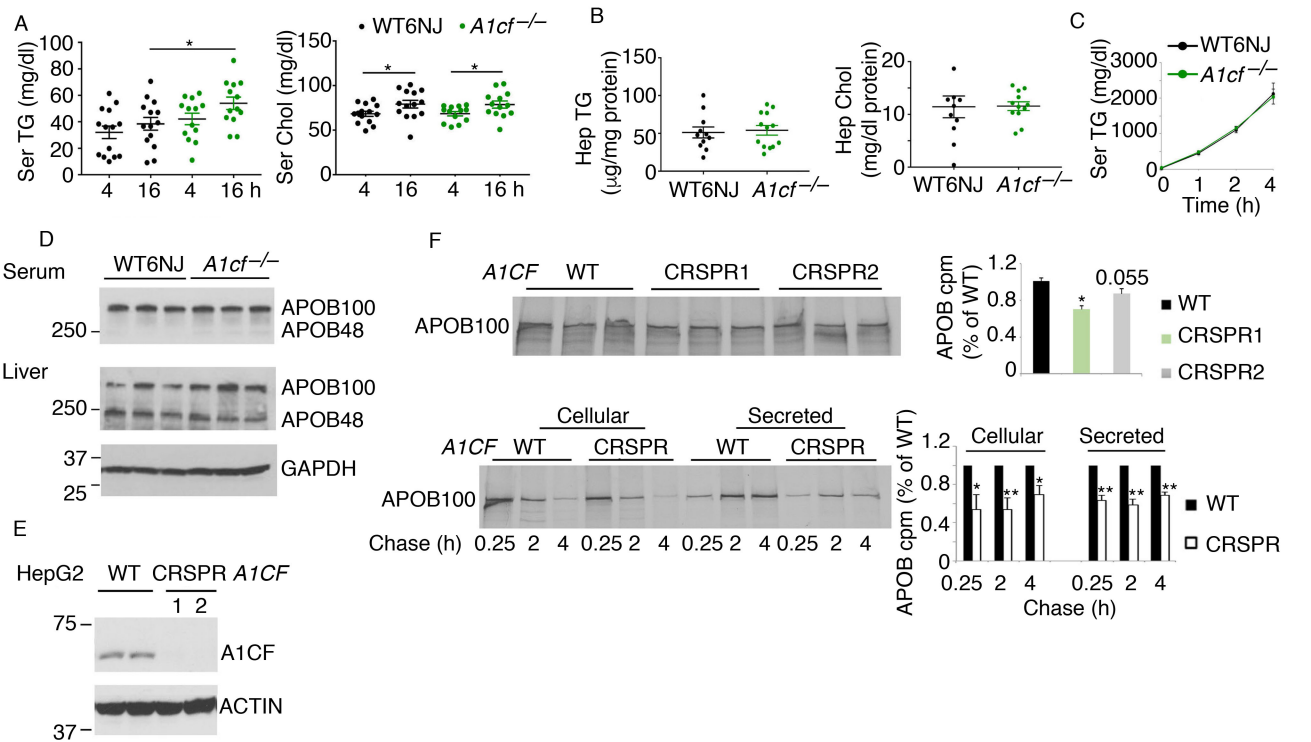

Supplemental Figure 2

Supplemental Figure 2. *A1cf* $^{-/-}$ mice show no alteration of APOB and VLDL secretion. (**A**) Serum TG and cholesterol in chow-fed *A1cf* $^{-/-}$ mice after a 4 or 16 h fast, n=13-14 animals per genotype and fasting condition. Data are means ± SE, * $P < 0.05$ (unpaired t-test). (**B**) Hepatic TG and cholesterol contents normalized to hepatic protein. Values are means ± SE from 11-13 mice per genotype. (**C**) Serum TG secretion rate in *A1cf* $^{-/-}$ mice following Pluronic F-127 injection after an overnight fast. Each point represents mean ± SE (n=6 per genotype). (**D**) Western blot analysis of serum and hepatic APOB after a 4h fast. GAPDH was used as loading control. (**E**) Western blot validation of A1CF knockout in two separate HepG2 CRSPR *A1CF* clones. ACTIN was used as loading control. (**F**) APOB synthesis in 2 separate HepG2 CRISPR *A1CF* clones. Following 15 min incubation with ^{35}S-methionine, extracts were separated on a 4-15% SDS-PAGE. After autoradiography radiolabeled APOB was quantitated by determination of count (cpm) in APOB protein band and expressed as % of WT CPM. Data represent mean ± SE (n=3 per clones). Cellular and secreted APOB was evaluated after pulse chase analysis. Autoradiograph is a representative image of two independent experiments, each performed with two separate HepG2 CRSPR *A1CF* clones. Quantitation of cellular and secreted APOB100 is shown in the graphical representation. Values for the HepG2 CRSPR *A1CF* represent mean ± SE (2 separate clones/ 2 independent experiments) * $P < 0.05$; ** $P < 0.01$ (unpaired t-test).

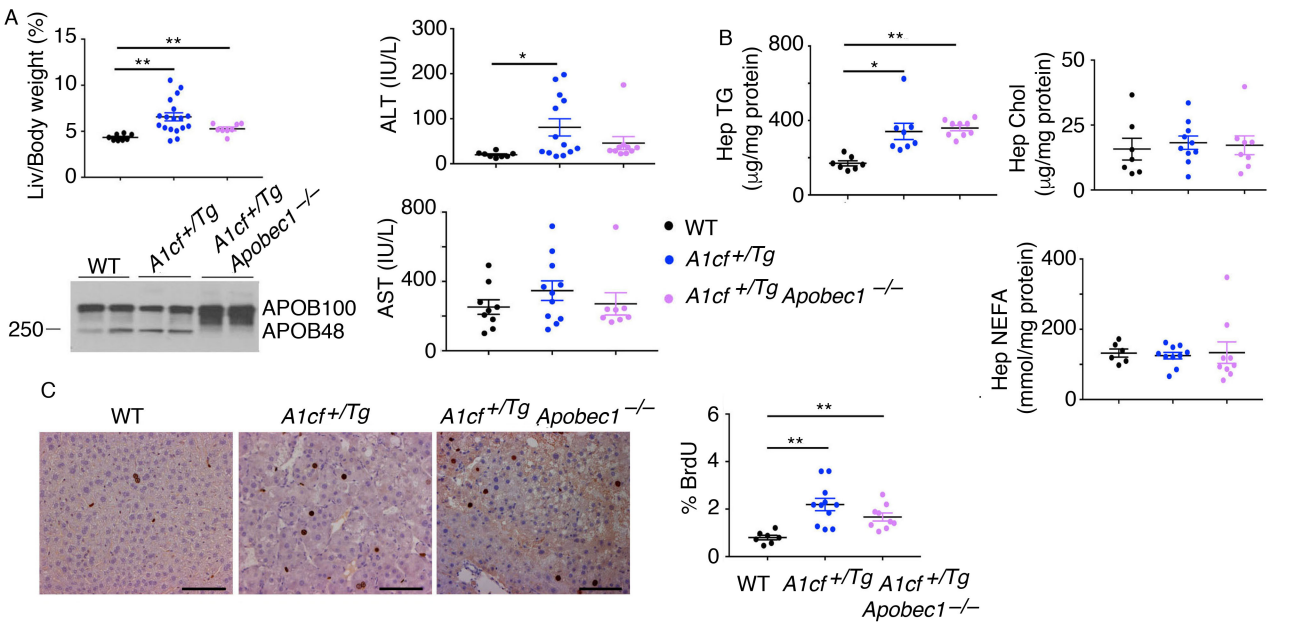

Supplemental Figure 3

Supplemental Figure 3. Characterization of chow-fed 12 month-old *A1cf* $^{+/Tg}$ mice. (**A**) Liver to body weight ratio of aged *A1cf* $^{+/Tg}$ (n=14) and *A1cf* $^{+/Tg}$ *Apobec1*$^{-/-}$ (n=10), represented as mean ± SE, ** $P < 0.01$ (Unpaired t-test for individual comparison with WT control). Significance between means of the 3 groups was determined using one-way ANOVA, P value = 0.0021). Plasma ALT and AST in aged *A1cf* $^{+/Tg}$ and *A1cf* $^{+/Tg}$ *Apobec1* $^{-/-}$ mice (n=7-13) as mean ± SE * $P < 0.05$ (Unpaired t-test). Significance between the 3 groups was determined using one-way ANOVA, P value = 0.0425. Lower panel, Western blot of APOB isoforms (B100 and B48) in serum of aged *A1cf* $^{+/Tg}$ and *A1cf* $^{+/Tg}$ *Apobec1* $^{-/-}$ mice. (**B**) Hepatic lipid in aged mice (n=7-10) represented as mean ± SE, * $P < 0.05$; ** $P < 0.01$ (Unpaired t-test for individual comparison with WT). Significance between the 3 groups was evaluated using one-way ANOVA, $P = 0.0002$). (**C**) Hepatocytes stained with BrdU in aged *A1cf* $^{+/Tg}$ and *A1cf* $^{+/Tg}$ *Apobec1* $^{-/-}$ livers and proliferative index expressed as percent of BrdU-positive hepatocytes. Data represent means ± SE (n=7-10) ** $P < 0.01$ (unpaired t-test for individual comparison). One-way ANOVA was used to determined significance between all groups, $P = 0.0006$). Scale bars: 50 μm.

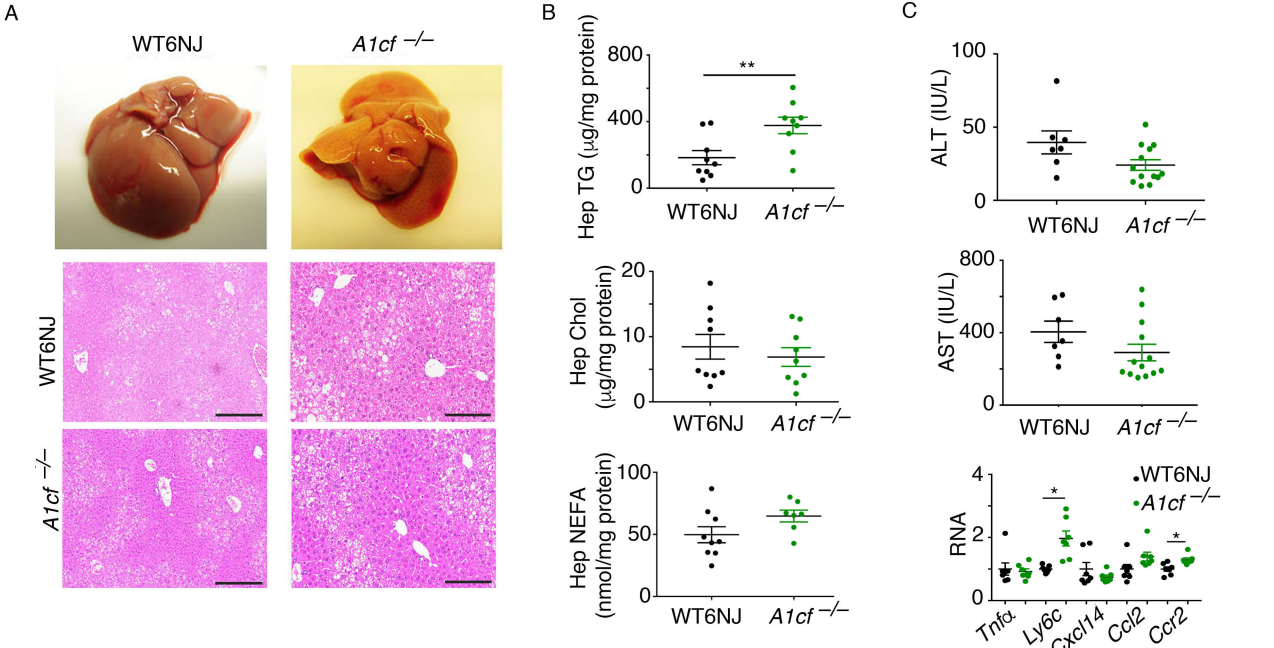

Supplemental Figure 4

Supplemental Figure 4. Chow-fed aged *A1cf* $^{-/-}$ do not develop spontaneous tumors. (**A**) Liver gross views and H&E sections from aged *A1cf* $^{-/-}$ mice. Scale bars: 100 μm (left) and 50 μm (right). (**B**) Hepatic lipid represented as mean ± SE, ** $P < 0.01$ (n=9) (Unpaired t-test). (**C**) Plasma ALT and AST in aged *A1cf* $^{-/-}$ mice shown as mean ± SE (n=7-13). QPCR determination of Inflammatory markers RNA expression in aged *A1cf* $^{-/-}$ liver represented as mean ± SE, * $P < 0.05$ (n=7) (Unpaired t-test).

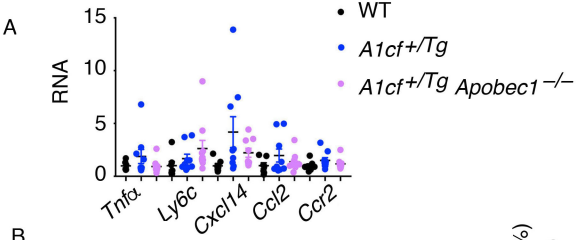

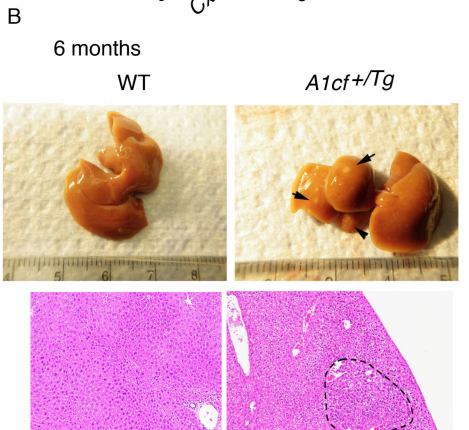

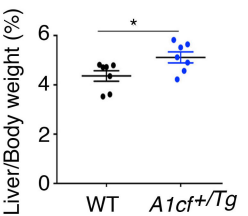

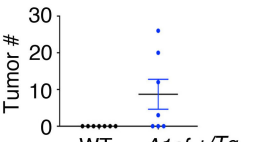

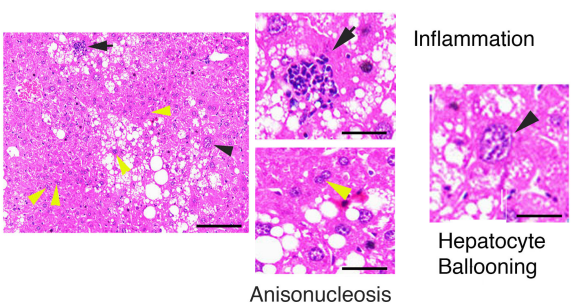

Supplemental Figure 5

Supplemental Figure 5. (**A**) QPCR evaluation of Inflammatory markers RNA expression in aged *A1cf* $^{+/Tg}$ and *A1cf* $^{+/Tg}$ *Apobec1* $^{-/-}$ (n=7) as mean ± SE. (**B**) Livers from 6-month-old chow-fed *A1cf* $^{+/Tg}$ and H&E staining of liver sections. The arrows indicate macroscopic tumors (dashed area). Scale bars: 100 μm. Liver to whole body weight ratio as mean ± SE (n=7) * $P < 0.05$ (Unpaired t-test). Tumor burden evaluated as number of macroscopically detectable tumors. Histological features of livers from 6-month-old chow-fed *A1cf* $^{+/Tg}$ mice. Black arrowheads: focal inflammation and hepatocyte ballooning. Yellow arrowheads: anisonucleosis. Scale bars: 50 μm.

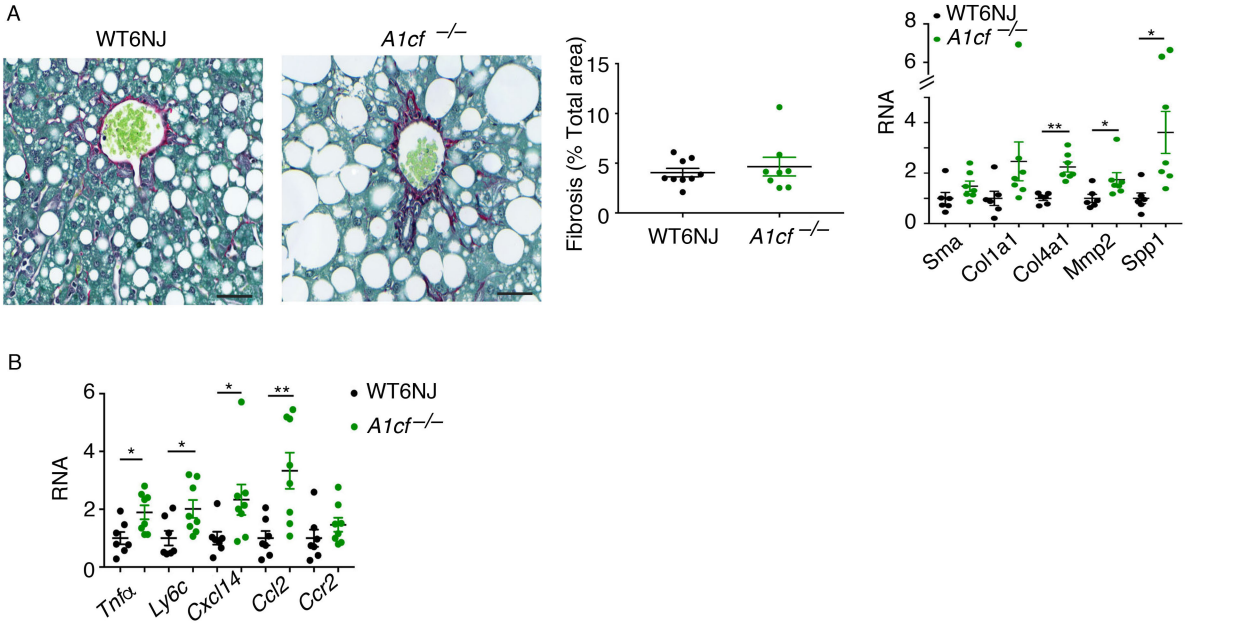

Supplemental Figure 6

Supplemental Figure 6. TFF-fed *A1cf* $^{-/-}$ mice exhibit similar fibrotic injury to WT controls but activation of inflammatory response. (**A**) Representative images of Sirius red staining of livers from *A1cf* $^{-/-}$ mice fed a TFF diet for 6 months. Scale bars: 20 μm. Sirius red-positive area was expressed as percent total area (n=8-9 animals per genotype) and represented as mean ± SE (n=8-9). Relative expression of fibrogenic genes evaluated by QPCR. Data represent mean ± SE (n=6-7 per genotype). Unpaired t-test was used to determine significance between *A1cf* $^{-/-}$ and WT6NJ RNA samples. * $P < 0.05$, ** $P < 0.01$. (**B**) Expression of inflammatory markers determined by QPCR. Data represent mean ± SE (n=6 -8 per genotype), * $P < 0.05$; ** $P < 0.01$ (Unpaired t-test).

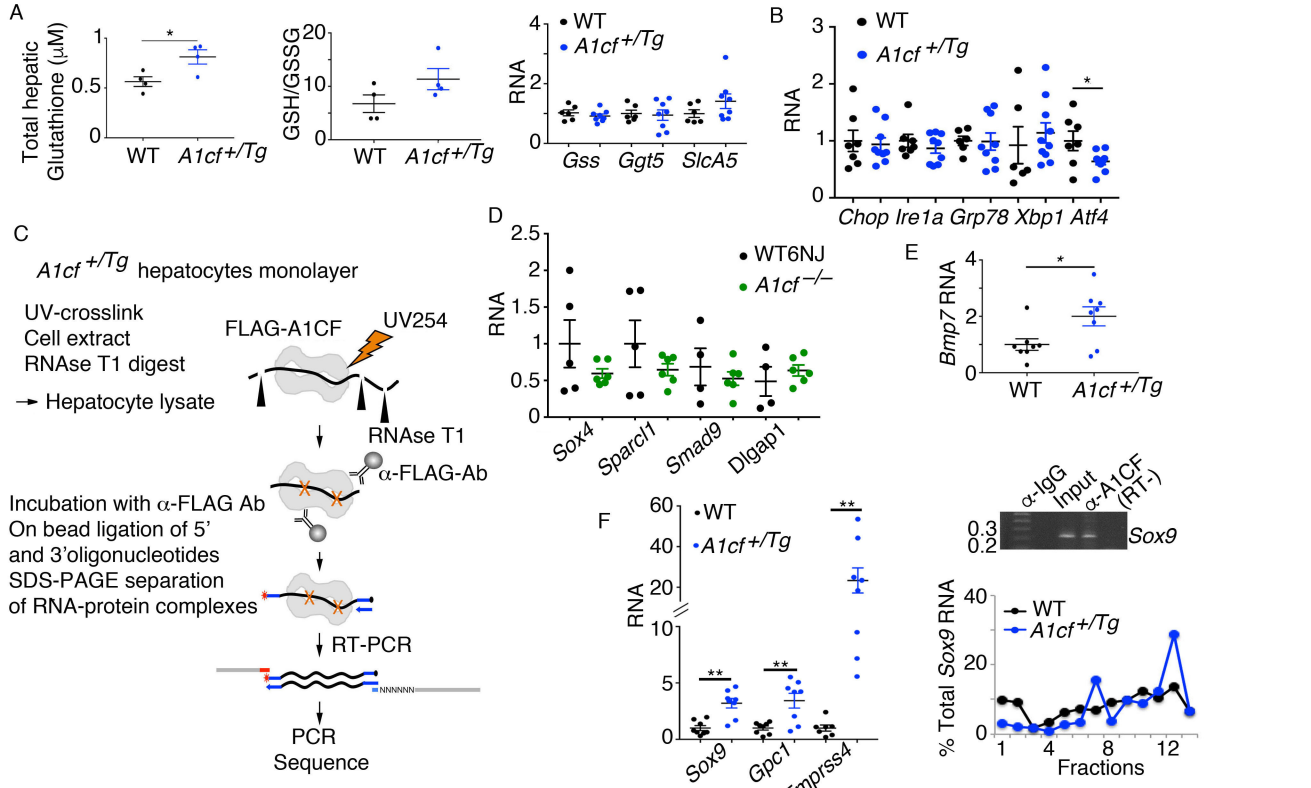

Supplemental Figure 7

Supplemental Figure 7. Oxidative stress characterization of young *A1cf* $^{+/Tg}$ mice. (**A**) Hepatic glutathione levels in WT and *A1cf* $^{+/Tg}$ liver. Levels of glutathione are represented both as total glutathione and as reduced to oxidized glutathione ratio. Data represent mean ± SE (n=4); * P< 0.05 (unpaired t-test). QPCR expression of RNAs involved in glutathione synthesis (*Gss*, *Slc1A5*) and transport (*Ggt5*) (6-8 animals per genotype). Data represent mean ± SE (unpaired t-test). (**B**) QPCR expression of ER-stress response related genes (6-9 animals per genotype). Data are mean ± SE, * P < 0.05 (unpaired t-test). (**C**) Schematic of RNA-CLIP method as described in Methods. (**D**) QPCR expression of A1CF RNA targets differentially expressed in 12-week-old *A1cf* $^{+/Tg}$ liver (see figure 9) in age-matched *A1cf* $^{-/-}$ livers. Data represent mean ± SE, (n= 5-6). (**E**) QPCR expression of *Bmp7* RNA in liver from young *A1cf* $^{+/Tg}$ mice, represented as mean ± SE (n=8); * P < 0.05 (unpaired t-test). (**F**) Left, Increased expression of RNAs involved in organogenesis in 12-week-old chow-fed *A1cf* $^{+/Tg}$ liver. QPCR from 7-8 animals per genotype. Data represent mean ± SE, * P < 0.05; ** P < 0.01 (unpaired t-test). Right top panel, representative image of 3 independent co-immunoprecipitations (IP) of A1CF and *Sox9* RNA from whole liver extract. Control immunoprecipitation with IgG was performed to confirm the specificity of anti-A1CF antibody. *Sox9* RNA was detected only in input fraction (total RNA before IP) and in the A1CF-specific IP. Right lower panel, polysomal distribution of *Sox9* RNA from sucrose gradient-fractionated hepatic cytoplasmic extracts isolated from *A1cf* $^{+/Tg}$. *Sox9* RNA in each fraction was analyzed by QPCR. Data are means of 2 separate isolations per genotype.

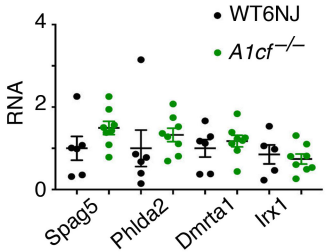

Supplemental Figure 8

Supplemental Figure 8. Gain/loss of function effect on differentially expressed A1CF RNA targets identified in 12 month-old *A1cf* $^{+/Tg}$ mice. Expression of A1CF RNA targets identified by RNA-Seq in aged *A1cf* $^{+/Tg}$ mice (Figure 12) was compared by QPCR in the aged *A1cf* $^{-/-}$ liver. Data represent mean ± SE, n= 5-8 animals per genotype (unpaired t-test).

A

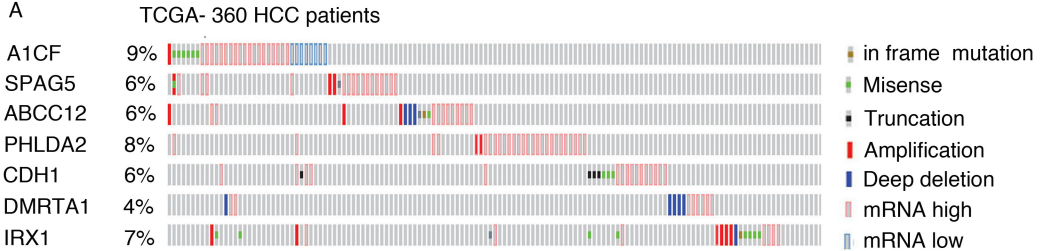

A1CF vs SPAG5 5/360 co-occurence p-value 0.031
A1CF vs CDH1 5/360 co-occurence p-value 0.054

B

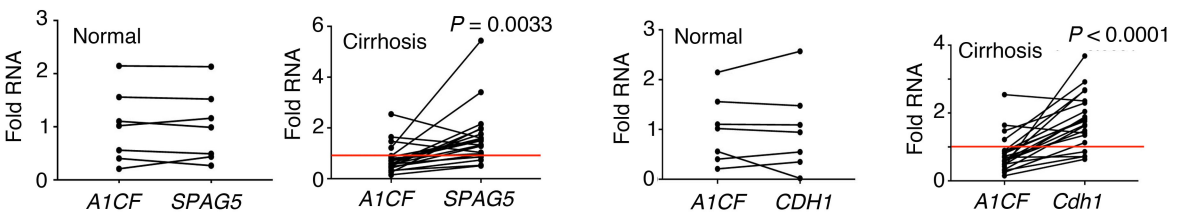

Supplemental Figure 9

Supplemental Figure 9. Expression of A1CF RNA targets in human HCC. (**A**) Oncoprint representing distribution of genetic alterations of A1CF RNA targets differentially expressed in 12-month-old *A1cf* $^{+/Tg}$ mice in 366 patients with liver hepatocellular carcinoma (HCC) from TCGA database (cbioportal.org). Genetic alterations are indicated to the right. The percentage associated with each gene indicates the number of patients with a genetic alteration of the given gene over the total number of profiled patients. Below the oncoprint are indicated two A1CF RNA-CLIP targets (*SPAG5*, *CDH1*) whose genetic alteration significantly co-occurs with A1CF alteration. (**B**) Comparison of expression of *A1CF*, *SPAG5* and *CDH1* RNAs in 21 cirrhotic human liver samples. Expression of individual RNAs by QPCR was evaluated in relation to 7 normal human livers. Fold expression in normal tissue is indicated as 1 (red line). Fold expression of *SPAG5* and *CDH1* RNAs was then separately compared to *A1CF* RNA among categories. *P* values are indicated on top of each graph (unpaired t-test).

Table 1. Pathological analysis of 12 month-old *A1cf* $^{+/Tg}$ livers.

	WT	*A1cf* $^{+/Tg}$	*A1cf* $^{+/Tg}$ *Apobec1*$^{-/-}$	WT6NJ	*A1cf* $^{-/-}$
# Animals	7	13	10	7	10
No lesion	7	1	0	7	10
Non dysplastic lesions	0	1	5	0	0
Dysplastic lesions	0	7	4	0	0
HCC	0	4	1	0	0

Table 2. Pathological analysis of livers of 6 month-old TFF fed *A1cf* $^{+/Tg}$.

	WT	*A1cf* $^{+/Tg}$	WT6NJ	*A1cf* $^{-/-}$
Animals	8	14	9	12
No lesion	8	5	9	12
Non Dysplastic lesions	0	2	0	0
Dysplastic lesions	0	7	0	0

Table 3. Distribution of patients by A1CF expression category in uninvolved and tumor tissue.

A1CF expression	Number of patients	
Category	Uninvolved	Tumor
1	39	36
2	45	36
3	23	30
4	20	35
Total	127	137

Supplemental Table S1. 3'UTR sequences of A1CF RNA targets identified by RNA-CLIP and differentially expressed in *A1cf* $^{+/Tg}$ mice.

Gene	Length (nt)	A	U	A and U	% AU	AUUUA	Poly(U) (5U)	Poly(U) > 6U
Sox4	2807	819	858	1677	59.74	4	>20	14 (+)
Sox9	2247	644	788	1432	63.73	6	>20	13 (+)
Sparcl1	441	151	138	289	65.53	0	0	0
Dlgap1	3179	976	920	1896	59.64	12	11 (+)	4 (+)
Smad9	3767	1105	1038	2143	56.9	8	9 (+)	3 (+)
Dram1	1937	536	557	1093	56.43	6	6 (+)	2 (+)
Phlda2	268	57	73	130	48.51	1	2 (+)	2 (+)
Cdh1	1647	446	490	936	56.83	2	8 (+)	4 (+)
Irx1	402	108	113	221	54.9	0	2 (+)	1 (+)
Dmrta1	2490	827	813	1640	65.9	6	10 (+)	1 (+)
Abcc12	377	95	85	180	47.74	0	0	0
Spag5	258	83	67	150	58.14	2	0	0

(+) represents one poly(U) motif with the indicated number of uridines

Supplemental Table S2. Clinical and laboratory data for all hepatocellular cancer patients.

Parameter	**N (%) / mean (±SD)**
Gender	
Female	51 (37%)
Male	86 (63%)
Age at diagnosis (year)	62.70 (±14.3)
Body mass index (kg/m^2)	27.71 (±5.7)
Obese (body mass index >30)	
No	91 (72%)
Yes	35 (28%)
Race	
Caucasian	96 (71%)
African American	4 (3%)
Asian	8 (6%)
Hispanic	2 (1.5%)
Unknown	25 (18.5%)
Underlying liver disease	
HCV hepatitis	27 (20%)
Alcoholic hepatitis	19 (14%)
NAFLD	19 (14%)
HBV hepatitis	13 (9%)
Alcoholic hepatitis and HCV hepatitis	2 (1%)
HBV and HCV hepatitis	1 (1%)
Other/Unknown	56 (41%)
Total follow-up (week)	193.3 (±184.6)
Survival by the end of follow-up	
Alive	17 (12%)
Dead	120 (88%)
Recurrence follow-up (week)	111.9 (±139.7)
Recurrence	
No	33 (30%)
Yes	77 (70%)
Eastern cooperative oncology group (ECOG) performance status	
0	77 (60%)
1	40 (31%)
2	10 (8%)
3	2 (1%)
Barcelona clinic liver cancer (BCLC) stage	
0	7 (5%)
1	46 (34%)
2	18 (13%)

3	60 (44%)
4	5 (4%)
Tumor, Node, Metastasis (TNM) stage	
1	90 (75%)
2	8 (7%)
3	14 (11%)
4	8 (7%)
Tumor number	
1	91 (67%)
2	17 (13%)
3	9 (7%)
>3	18 (13%)
Extent of liver fibrosis	
0	45 (34%)
1	5 (4%)
2	9 (7%)
3	4 (3%)
4	70 (52%)
Alpha Fetoprotein (ng/mL)	23486.18 (±184510.10)
Alkaline phosphatase (IU/L)	263.29 (±346.1)
Aspartate aminotransferase (IU/L)	84.39 (±84.1)
Alanine transaminase (IU/L)	79.23 (±83.2)
Sodium (mEq/L)	139.08 (±3.6)
Prothrombin time (seconds)	1.09 (±0.2)
White blood cell (count/μL)	6442.86 (±2990.8)
Hemoglobin (g/dL)	13.26 (±1.7)
Platelet (count/μL)	212.00 (±130)
Total bilirubin (mg/dL)	1.20 (±1)
Creatinine (mg/dL)	1.13 (±1)
Albumin (g/dL)	3.71 (±0.6)
Child-Pugh score	5.83 (±1.4)
Model for end-stage liver disease (MELD) score	9.42 (±3.72)
SD: standard deviation; HCV: hepatitis C virus; HBV: hepatitis B virus; NAFLD: non-alcoholic fatty liver disease; IU: international unit; mEq: milliequivalent.	

Supplemental Table S3. Multivariable Cox proportional-hazard model for overall survival of hepatocellular cancer patients.

Prognostic factor	subgroups	Hazard ratio	P value
Eastern cooperative oncology group (ECOG) performance status	0	Reference	
	1	1.45	.2
	2	5.38	<.001
Alkaline phosphatase (IU/L)	per 100-unit increments	1.05	<.001
White blood cell (count per μL)	per 1000-unit increments	1.09	.09
Tumor number	1	Reference	
	2	1.17	.66
	3	3.38	.02
	>3	1.04	.88
TNM stage	1	Reference	
	2	0.53	.35
	3	2.70	.003
	4	2.17	.06
Total A1CF expression	quartile 1	Reference	
	quartile 2	1.55	.14
	quartile 3	1.66	.05
	quartile 4	2.01	.05

TNM: tumor, node, metastasis; A1CF: APOBEC1 complementation factor

Supplemental Table S4. Clinical and laboratory data for hepatocellular cancer patients with underlying NAFLD.

Parameter	**N (%) / mean (±SD)**
Gender	
Female	5 (26%)
Male	14 (74%)
Age at diagnosis (year)	65.71 (±10.5)
Race	
Caucasian	17 (89%)
Unknown	2 (11%)
Body mass index (kg/m^2)	34.01 (±4.7)
Obese (body mass index >30)	
No	2 (11%)
Yes	16 (89%)
Total follow-up (week)	188.64 (±146.8)
Survival	
Alive	3 (16%)
Dead	16 (84%)
Recurrence follow-up (week)	85.0 (±84.6)
Recurrence	
No	5 (28%)
Yes	13 (72%)
NAFLD: non-alcoholic fatty liver disease; SD: standard deviation	

Supplemental Table S5. Multivariable Cox proportional-hazard model for overall survival of hepatocellular cancer patients with underlying NAFLD.

Prognostic factor	subgroups	Hazard ratio	P value
Time to the first recurrence (week)	per 1-unit increments	0.99	.03
Recurrence	No	Reference	
	Yes	1.41	.7
Total A1CF expression	Quartile 1	Reference	
	Quartile 2	2.0	.5
	Quartile 3	8.10	.01
	Quartile 4	8.64	.002

NAFLD: non-alcoholic fatty liver disease; A1CF: APOBEC1 complementation factor

Supplemental Table S6. Demographic descriptors for Hong Kong patient cohort.

cDNA	Sex/Age	Diagnosis
306N	F/46	CA colon to liver, Metastatic adenocarcinoma
209N	M/43	CA colon to liver, Metastatic adenocarcinoma
215N	F/44	CA colon to liver, Metastatic adenocarcinoma
422N	F/31	CA colon to liver, Metastatic adenocarcinoma
227N	F/48	CA colon to liver, Metastatic adenocarcinoma
279N	M/69	Autopsy. COD: Ruptured abdominal aortic aneurysm. Sever coronary atherosclerosis with acute myocardial infraction
335N	M/53	CA colon to liver, Metastatic adenocarcinoma
C441	F/51	Explanted liver, High grade dysplastic nodule, macroregenerative nodules; HBV-associated cirrhosis, chronic cholecystitis; cholelithiasis.
C440	M/40	Explanted liver, HBV-associated cirrhosis, fatty change with Mallory bodies
C456	M/49	Explanted liver, Active HBV-associated cirrhosis
C231	M/39	Explanted liver, Fibrosing cholestatic hepatitis
C453		Explanted liver, HBV-associated cirrhosis, moderate activity, large regenerative nodules, chronic cholecystitis, cholelithiasis
C452	M/49	Explanted liver; HBV-associated cirrhosis with severe activity, macroregenerative nodules
ch281	M/55	Explanted liver. Cirrhosis in keeping with chronic Hep B
ch253	M/49	Explanted liver, chronic Hep B virus associated cirrhosis with acute exacerbation: Cholestasis
ch229	M/47	Explanted liver, Chronic hepatitis in a background of cirrhosis (Scheuer grade 2, Stage 4), regenerate nodules formation
ch279	M/40	Explanted liver. Chronic Hepatitis, grade 3 Stage 4 cirrhosis.
ch261	M/52	Explanted liver, Cirrhosis, compatible with HBV-related
ch277	M/43	Explanted liver. Chronic Hep B cirrhosis: mild haemosiderosis
ch329	F/55	Explanted liver. Cirrhosis. Portal vein thrombus.
ch263	M/57	Explanted liver, Submassive hepatic necrosis: chronic Hep B with bridging fibrosis
ch361	M/55	Explanted liver. Cirrhosis and Hep B with siderosis
ch246	M/61	Explanted liver, Hep B associated cirrhosis
ch230	M/58	Explanted liver. Irregular cirrhosis with no malignancy

ch295	M/46	Explanted liver. Hep B associated mild chronic Hepatitis with cirrhosis. Chronic cholecystitis
ch297	F/61	Explanted liver. Chronic Hep B with septal fibrosis & minimal activity; portal vein thrombosis
ch294	M/49	Explanted liver, HBV-associated cirrhosis, with mild activity, grade 2-3 siderosis. Caroli's disease
ch225	M/49	Explanted liver, alcoholic cirrhosis, liver flukes

Supplemental Table S7. Antibodies.

Antibodies	Species	Manufacturer	Catalog #	WB	IH
A1CF	Rabbit	*		1:3000	1:2000
FLAG	Rabbit	ThermoScientific	PA1-984B	1:1000	1:200
CIDEA	Rabbit	Millipore	ABC350	1:600	1:100
β-CATENIN	Mouse	BD Biosciences	610154	1:2000	1:600
CDH1	Mouse	Abcam	76055		1:250
CYCLIN D1	Rabbit	Abcam	134175		1:100
HSP70	Rabbit	Abcam	2787		1:200
GPC3	Mouse	ThermoScientific	1G12		1:100
P62	Rabbit	Millipore	EP396		1:200
APOB	Rabbit	**		1:4000	
CD36	Goat	R&D	AF2519	1:7000	
MOGAT1	Rabbit	***		1:1000	
MOGAT2	Rabbit	Invitrogen	PA5-42625	1:1000	
ACTIN	Rabbit	Sigma	A2066	1:2000	
GAPDH	Rabbit	Santa Cruz Biotechnology	Sc-25778	1:1000	
STAT3	Mouse	Cell Signaling	9139S	1:2000	
PSTAT3	Rabbit	Cell Signaling	9131S	1:1000	

* (67); ** (68)*** (69)

Supplemental Table S8. Quantitative PCR primers.

RNA	Forward primer	Reverse Primer
Abcc12	5'-GAGGAGTTCAGGAGCTCAAGCA-3'	5'-AGACCCTGTATGGAGGAGGTGAT-3'
αfp	5'-TCATGTATGCCCCAGCCATT-3'	5'-CAGCATGCCAGAACGACCTT-3'
Apob	5'-AATATAATCGGAGAAGCAGGACCTA-3'	5'-TCCCGAAGTTGACATCAAACC-3'
αSma	5'-CCAGAGCAAGAGAGGGATCCT-3'	5'-TGTCGTCCCAGTTGGTGATG-3'
Atf4	5'-CGAGTTAAGCACATTCCTGGAATC-3'	5'-TTCGCTGTTCAGGAAGCTCAT-3'
Bmp7	5'-CCTTCATGGTGGCCTTCTTC-3'	5'-CCCCGTGGACCGGATACTA-3'
Cbr3	5'-AGAGGAAAGCGGACAGGATTC-3'	5'-TCGCCATGTCGGTCTTCA-3'
Ccr2	5'-TCCACGGCATACTATCAACATCTC-3'	5'-GGCCCCTTCATCAAGCTCTT-3'
Cdh1	5'-ACCCCCTTACGACTCTCTGTTG-3'	5'-CAGGCTAGCGGCTTCAGAAC-3'
Cdh24	5'-CGTACAGCCATCCCCAACAT-3'	5'-GCTTGAATCACCACCAAGAACTC-3'
Cdk1	5'-GGACGAGAACGGCTTGGAT-3'	5'-ATTCGTTTGGCAGGATCATAGAC-3'
Cd36	5'-TCTTCCAGCCAATGCCTTTG-3'	5'-TGGAGATTACTTTTTCAGTGCAGAA-3'
Chka	5'-GGTCACTTGGGCCAAAACTC-3'	5'-CGCCGGCTCGGGATA-3'
Chop	5'-CCACCACACCTGAAAGCAGAA-3'	5'-TGAAAGGCAGGGACTCA-3'
Cidea	5'-CCAGAGTCACCTTCGACCTATACA-3'	5'-CATCGTGGCTTTGACATTGAGA-3'
Col1a1	5'-CACGGCTGTGTGCGATGA-3'	5'-TCGCCCTCCCGTCTTTG-3'
Col4a1	5'-CCAGGATGCAACGGTACAAA-3'	5'-AACGTGGCCGAGAATTTCAC-3'
Cxcl14	5'-GCACTGCCTGCACCCTAAG-3'	5'-TCGTTCCAGGCATTGTACCA-3'
Dlgap1	5'-GCAGCCGATGACGACTTTG-3'	5'-GTCCGGAGGAGGCAGGATAG-3'
Dmrta1	5'-CTGGTTCCAGCATTGCCTTT-3'	5'-ATCATCCCTGGAAACGCATAA-3'
Dram1	5'-GCCATCTCCGCTGTTTCGT-3'	5'-GGATTCCATTCCAGCTTGGTT-3'
Gapdh	5'-TGTGTCCGTCGTGGATCTGA-3'	5'-CCTGCTTCACCACCTTCTTGA-3'
Ggt5	5'-GGTTCCCGTGTGCCCTTTATC-3'	5'-GCCGCAGGATGCTGTTGT-3'
Gpc1	5'-GGACATCACCAAGCCAGACA-3'	5'-CATAGGCGCCACGTAAACG-3'
Gpx3	5'-TCACCTGGCCGCCTCTT-3'	5'-AAAGTTCCAGCGGATGTCATG-3'
Grp78	5'-ACCCCGAGAACACGGTCTT-3'	5'-GCTGCACCGAAGGGTCATT-3'
Gss	5'-CATTGCCCAGACCGTGTTC-3'	5'-TGCGCCGCACTGGAA-3'
Gstm3	5'-TGCTGCAGTCCCGATTTTG-3'	5'-TTCTCAGGGATGGCCTTCAA-3'
Il19	5'-GACATGCGCCTCATAGAAAAGA-3'	5'-ACAGGATGGTGACATTTTTAAAGGT-3'
Jak3	5'-TGCTGCCCTGAACCTAACATC-3'	5'-TTCGCACCACGATCAAATTG-3'
Kif20a	5'-ACCTAGCCATCAGCATAAGAGACA-3'	5'-CACGTAAGGATTGCCGTTCTG-3'
Klf4	5'-ACCTATACCAAGAGTTCTCATCTCAA3'	5'-CCGTCCCAGTCACAGTGGTAA-3'
Ly6c	5'-GGATTCTGCATTGCTCAAAACA-3'	5'-CTGACGGGTCTTTAGTTTCCTTCT-3'
Mcm2	5'-GTTCAGCGTCATGCGGAGTAT-3'	5'-TCTCGCCGGAAGGAGAGATA-3'
Mcm4	5'-CCAACCCAGTCCCTTCGAA-3'	5'-TCGCCTCTACGTCTCCGATT-3'
Mcm6	5'-TGTCAGCGCCCATCATGT-3'	5'-CATTGCATTCATCCACCAGAA-3'
Mmp2	5'-CTATGTCCACTGTGGGTGGAAA-3'	5'-TTGTTGCCCAGGAAAGTGAAG-3'
Mogat1	5'-ACCACAAATCCTGCGAAAGG-3'	5'-TGTTGAGTGGCGCGAACTC-3'
Mogat2	5'-CTGATGATGCTGACTGTGTGGTT-3'	5'-CCAGCCCCCCAGACATG-3'

Pbrm1	5’-GGTGTTACAGCGACTCCTTAGCA-3’	5’-CCGATACCGATTACTTTCAACATTT-3’
Phlda2	5’-ACCGCCTGCGCCTCTT-3’	5’-TGGAGTGGAAAAAACAGCTCCTT-3’
Rb1	5’-TCCACCAGGCCTCCTACCT-3’	5’-GAATCCGTAAGGGTGAACTAGAAAAC-3’
Sall2	5’-TCCACCTTCGTTCCCACACT-3’	5’-CCGAGTTGTGAAACGGTTACC-3’
Scd2	5’-GTACCGCTGGCACATCAACTT-3’	5’-ACACTCTCTTCCGGTCGTAAGC-3’
Slc1a5	5’-GCCAGCAAGATTGTGGAGATG-3’	5’-TGTATTTGCCGAGGCTGATG-3’
Smad9	5’-AAAACACCAGGAGGCACATTG-3’	5’-ACCTCGCCCCCAACGTA-3’
Sox4	5’-GGCTAGGCAAACGCTGGAA-3’	5’-TCCTGGATGAACGGAATCTTG-3’
Sox9	5’-CGGCTCCAGCAAGAACAAG-3’	5’-TGCGCCCACACCATGA-3’
Spag5	5’-TTGCAGCAGGACTGGACATC-3’	5’-TCGAGACCAACTCAGCAAAGC-3’
Sparcl1	5’-CTCGCTTCTTTGAGGAGTGTGA-3’	5’-TGGCCCCATTCCTTCAAG-3’
Spp1	5’-TTTCACTCCAATCGTCCCTACA-3’	5’-TCAGTCCATAAGCCAAGCTATCAC-3’
Tmp1	5’-CATGGAAAGCCTCTGTGGATATG-3’	5’-GATGTGCAAATTTCCGTTCCTT-3’
Tmprss4	5’-CCTGCAGACAGATGGGCTATG-3’	5’-GGTTCTGATCTGGACGGATCTC-3’
Tnf α	5’-TACCTTGTCTACTCCCAGGTTCTCT-3’	5’-GTGTGGGTGAGGAGCACGTA-3’
Xbp1	5’-ATCAGCTTTTACGGGAGAAAACTC-3’	5’-CCATTCCCAAGCGTGTTCTT-3’
Xpo4	5’-GCAGTGCCTTGCCCAGTT-3’	5’-AATCAACCTGGGATCCTTCGT-3’